# Autophagy Proteins Promote Repair of Endosomal Membranes Damaged by the Salmonella Type Three Secretion System 1

Kreibich, Saskia ; Emmenlauer, Mario ; Fredlund, Jennifer ; Rämö, Pauli ; Münz, Christian ; Dehio, Christoph ; Enninga, Jost ; Hardt, Wolf-Dietrich

Abstract: Salmonella Typhimurium (S.Tm) is an enteropathogen requiring multiple virulence factors, including two type three secretion systems (T1 and T2). T1 triggers epithelium invasion in which the bacteria are taken up into endosomes that mature into Salmonella-containing vacuoles (SCV) and trigger T2 induction upon acidification. Mechanisms controlling endosome membrane integrity or pathogen egress into the cytosol are incompletely understood. We screened for host factors affecting invasion and SCV maturation and identified a role for autophagy in sealing endosomal membranes damaged by T1 during host cell invasion. S.Tm-infected autophagy-deficient (atg5(-/-)) cells exhibit reduced SCV dye retention and lower T2 expression but no effects on steps preceding SCV maturation. However, in the absence of T1, autophagy is dispensable for T2 induction. These findings establish a role of autophagy at early stages of S.Tm infection and suggest that autophagy-mediated membrane repair might be generally important for invasive pathogens and endosomal membrane function.

DOI: https://doi.org/10.1016/j.chom.2015.10.015

# Autophagy proteins promote repair of endosome membranes damaged by *Salmonella* Type Three Secretion System 1

Saskia Kreibich[1], Mario Emmenlauer[2], Jennifer Fredlund[4], Pauli Rämö[2], Christian Münz[3], Christoph Dehio[2], Jost Enninga[4] and Wolf-Dietrich Hardt[1*]

[1]Institute of Microbiology, Swiss Federal Institute of Technology ETH Zurich, Switzerland; [2]Biozentrum, University of Basel, Switzerland; [3]Institute of Experimental Immunology, University of Zurich, Switzerland; [4]Dynamics of host-pathogen interaction Unit, Institut Pasteur Paris, France
*correspondence: hardt@micro.biol.ethz.ch

# Summary

*Salmonella* Typhimurium (*S*.Tm) is an enteropathogen requiring multiple virulence factors, including two type III secretion systems (T1, T2). T1 triggers epithelium invasion, while T2 is induced within "*Salmonella*-containing vacuoles" (SCV). Some bacteria escape into the cytosol and get eliminated by autophagy. Mechanisms controlling endosome membrane integrity or pathogen egress into the cytosol are incompletely understood. We used HeLa cell infections, *S*.Tm expressing a transcriptional T2-*gfp* reporter and siRNAs to screen for host cell factors controlling SCV maturation. This identified a novel role for autophagy in sealing damaged SCVs. Autophagy-deficient (*atg5*$^{-/-}$) cells, marker assays and pathogen quantification established that autophagy enhances repair of the endosome damage inflicted by T1 during host cell invasion. Thereby, autophagy promotes SCV maturation and boosts T2-expression. This establishes a novel role of autophagy at early stages of *S.*Tm infection. Autophagy-mediated membrane-repair might be of general importance for invasive pathogens and endosomal membrane function.

# Introduction

*Salmonella enterica* serovar Typhimurium (*S.*Tm) can cause diarrhea by infecting the gut tissue. This is facilitated by virulence factors, i.e. the type three secretion systems T1 and T2 which inject "effector proteins" and thereby manipulate host-cell responses (Kaiser et al., 2012). However, the precise role of T1 and T2 in the pathogen-host interaction and the mechanisms maintaining host cell membrane integrity in face of T1 and T2 are not yet fully understood.

The T1 effector proteins SipA, SopE, SopE2 and SopB trigger actin rearrangements and epithelial cell invasion (Table S1A; (Kaiser et al., 2012)). Initially, *S*.Tm lodges in endosomes. In wildtype (wt) epithelial cells, most *S*.Tm remain in "*Salmonella*-containing vacuoles" (SCV), which sequentially acquire early (Rab5) and late (Rab7, Rab9 and Lamp1) endosomal markers, acidify (thus triggering T2) but do not fuse with lysosomes (Bakowski et al., 2008; Smith et al., 2005; Yu et al., 2010). However, a small sub-fraction egresses from the SCV and grows at high rates in the host cell cytosol ("hyper-replication", (Knodler et al., 2014; Knodler et al., 2010; Malik-Kale et al., 2012)). It is still not completely understood how SCV egress and cytosolic hyper-replication are limited by the host cell.

Innate defenses allow mammalian cells to recognize and respond to bacteria (Fredlund and Enninga, 2014). This includes autophagy. Autophagy proteins promote cellular homeostasis by delivering cytosolic cargo to lysosomal degradation. Starvation, stress and intracellular bacteria can induce autophagy (Huang and Brumell, 2014), trigger the uptake of cytosol- and phagophore-residing pathogens into autophagosomes and target them for lysosomal pathogen elimination (Levine et al., 2011; Nakagawa et al., 2004; Shahnazari et al., 2011; Watson et al., 2012). Some pathogens can escape autophagic recognition (*L. monocytogenes*, *S. flexneri*) or subvert autophagy to their own benefit (*C. burnetii*, *F. tularensis, B. abortus*) (Baxt et al., 2013; Beron et al., 2002; Gutierrez et al., 2005; Ogawa et al., 2005; Romano et al., 2007; Starr et al., 2012; Yoshikawa et al., 2009). Thus, autophagy can impose important checkpoints for infection. However, the underlying mechanisms remain incompletely understood.

Autophagy can restrict *S*.Tm infections (Huang and Brumell, 2014). Most work employed bulk assays and thereby focused on T1-mediated SCV damage/egress, cytosolic hyper-replication and the mechanisms activating autophagy. Ruptured SCVs are sensed by galectins, cytoplasmic lectins recognizing carbohydrate modifications within the ruptured SCV, which subsequently recruit adaptors and autophagosomes (Thurston et al., 2012). Moreover, autophagy targets cytoplasmic *S*.Tm for degradation (Thurston et al., 2009; Thurston et al., 2012; Wild et al., 2011; Zheng et al., 2009). Thereby, dysfunctional autophagy leads to hyper-replication within the host cytoplasm (Birmingham et al., 2006; Kuballa et al., 2008; Tattoli et al., 2012). However, some contradictory evidence has been reported (Yu et al., 2014) and the precise role of autophagy in the infection is still not completely understood.

We employed an unbiased approach and a SCV-specific reporter to identify host cellular factors affecting the *S*.Tm infection process. This revealed a novel role for autophagy in the repair of T1-mediated SCV membrane damage.

# Results

## RNAi screen identifies host cell factors affecting *S*.Tm infection

To identify host cell factors affecting *S.*Tm infection, we conducted a genome-wide RNAi screen (GWS), using the "modified gentamicin-protection assay" (termed "*gfp*-reporter assay" from here on) and *S.*Tm$^{SopE}$, as described (Fig. 1A; Table S1A; (Misselwitz et al., 2011a)). *S.*Tm$^{SopE}$ (SL1344, Δ*sopE2sipAsopB*), which strictly requires SopE for host cell invasion (Schlumberger and Hardt, 2006), carried p*ssaG*, a reporter plasmid expressing GFP from a T2 promotor (Schlumberger et al., 2007). Thus, GFP is induced only after invasion of the host cell, when the pathogen arrives in a properly matured SCV (Fig. 1A; Fig. S1A-D; Suppl. Exp. Proc.; Fig. S6). Automated microscopy and image analysis quantified the "percentage of cells harboring T2-*gfp*$^+$ *S*.Tm". Thereby, host cell factors affecting any step of the infection pathway leading to SCV maturation could be identified, i.e. binding, effector translocation, ruffling, internalization, and the maturation of the SCV (Fig. S1A-D; (Misselwitz et al., 2011a)).

HeLa CCL-2 cells were transfected with a genome-wide siRNA library (Dharmacon ON-TARGETplus SMART pool; 18.237 target genes; 3 independent replicates), kinase/phosphatase-targeting or customized siRNA libraries (Table S1B) and infected for 4h. Infection efficiencies were scored by an automated image analysis pipeline (1000-3500 cells/well; Fig. 1B,C; Suppl. Exp. Proc.). "Biological" siRNA controls (Kif11, ArpC3, Cdc42) served as controls to verify plate quality and high inter-screen reproducibility ($R^2$ = 0.8 - 0.9; data not shown; (Misselwitz et al., 2011a) (Fig. S1E,F)).

Phenotypic clustering and mapping of the 5000 strongest hits (z-score ≤ -0.5; i.e. ≥ 30% attenuation) onto KEGG pathways identified signaling modules of interest. This "re-discovered" actin cytoskeleton regulators (e.g. Rac1, Cdc42, N-WASP, CYFIP2, NCKAP1, ABI2, WAVE2, Arp2/3 proteins, PFN; Fig. S1G), the COPI complex (Misselwitz et al., 2011a), the trafficking GTPases Rab5 and Rab7 and the vacuolar ATPases promoting SCV acidification and T2 induction (Rathman et al., 1996) (Table S1B). Strikingly, we also identified numerous strong autophagy hits affecting "Regulation and Recruitment", "Autophagy Initiation", and the "ATG12"- or the "ATG8" -conjugation system (Fig. 1D-H). Their silencing had only minor effects on the cell numbers (<<2-fold; Table S1B) and this effect did not affect our readout (data not shown). Some autophagy proteins (e.g. ATG10, ATG13, FIP200,) did not yield significant phenotypes. Most likely, this is explained by inefficient knockdown and/or masking by "positive" off-target effects (Franceschini et al., 2014). The ATG8-conjugation system yielded only subtle effects on *S*.Tm infection. It seems likely that this is explained by functional redundancy. Overall

however, silencing of most autophagy proteins reduced the number of cells harboring T2-*gfp*-expressing *S*.Tm. This phenotype was apparently at odds with the established role of autophagy in restricting cytosolic pathogen growth ((Birmingham et al., 2006); Fig. S2A,B) and it was not explained by autophagy-controlled pathogen expulsion (Fig. S2E,F). Thus, autophagy may have an additional function in the infection process which had not been discovered so far.

## *atg5*-deficient murine fibroblasts verify the need for autophagy in SCV maturation

Mouse embryonic fibroblasts (MEF) and an *atg5*$^{-/-}$ mutant (Kuma et al., 2004) were used to decipher the role of autophagy in SCV maturation and T2 induction. ATG5, ATG12 and ATG16L1 form an E3-ubiquitin ligase of the ATG8-conjugation system involved in autophagosome elongation and closure (Fujita et al., 2008; Hanada et al., 2007; Mizushima et al., 2003; Mizushima et al., 2001). When infected with *S*.Tm$^{SopE}$, T2-*gfp* expression was reduced by 50% in the *atg5*$^{-/-}$ cells ($p << 0.05$; Fig. 2A). Equivalent data were obtained in infections with wt (*S*.Tm; Fig. S2G) or *S*.Tm$^{SipA}$, an isogenic mutant invading via SipA (data not shown). This confirmed that the *atg5* phenotype is not limited to *S*.Tm$^{SopE}$, but of general relevance for *Salmonella* host cell infection.

## Infection steps preceding endosome/SCV maturation do not require *atg5*

Infection-stage-specific assays were used to map the effect of *atg5* deficiency. Docking, as measured by infecting *atg5*$^{-/-}$ and *atg5*$^{+/+}$ MEF for 6 min with *S*.Tm$^{\Delta 4}$ (lacks *sopE*, *sopE2*, *sopB*, *sipA*; docks via T1 and type I fimbriae; (Misselwitz et al., 2011b)) did not differ significantly between *atg5*$^{-/-}$ and *atg5*$^{+/+}$ MEF ($p \geq 0.05$; Fig. 2B). Equivalent observations were made in HeLa CCL-2 cells (log2 docking index 0.5 to -0.5; Fig. S2I). Also membrane ruffling, as analyzed 12 min p.i. with *S*.Tm$^{SopE}$, did not differ between *atg5*$^{-/-}$ and *atg5*$^{+/+}$ MEF ($p \geq 0.05$; Fig. 2C; Suppl. Exp. Proc.). Finally, at 1h p.i. a classical gentamicin-protection assay yielded equivalent levels of *S*.Tm$^{SopE}$ host cell invasion in *atg5*$^{-/-}$ and *atg5*$^{+/+}$ MEF ($p>0.05$; Fig. 2D). Thus, autophagy does not affect the steps preceding endosome/SCV maturation.

## Different kinetics of autophagy-promoted T2-induction and cytosolic hyper-replication

To delineate the onset of autophagy-promoted SCV maturation, *atg5*$^{-/-}$ and *atg5*$^{+/+}$ MEF were infected for 1-12h with *S*.Tm$^{SopE}$ (Fig. 2E). T2-*gfp* was expressed as early as 2h p.i. and *atg5*$^{-/-}$ cells revealed reduced induction levels ($p < 0.05$; Fig. 2E). Equivalent observations were made in wt *S*.Tm (Fig. S2G). In contrast, a classical gentamicin-protection assay yielded the well-described hyper-proliferation in *atg5*$^{-/-}$ cells. This assay detects "all" intracellular *S*.Tm, no matter whether they express T2-*gfp* or not.

As expected, the phenotype appeared later, i.e. by ≥ 4h p.i. ((Birmingham et al., 2006); Fig. 2F, Fig. S2A,B). After 5-6h, *atg5*$^{-/-}$ (but not the *atg5*$^{+/+}$) cells showed massive intracellular pathogen growth (Fig. 2G; (Brumell et al., 2002; Knodler et al., 2014; Knodler et al., 2010; Malik-Kale et al., 2012)). This was confirmed by fluorescence microscopy (Fig. S2J,K). Thus, cytoplasmic hyper-proliferation (at ≥ 4h p.i.) begins about 2h later than the autophagy-promoted SCV maturation (1-2h p.i.). Moreover, T2-*gfp*$^{+}$ *S*.Tm were still observable in *atg5*$^{-/-}$ cells harboring massive amounts of hyper-proliferating (T2-*gfp*$^{-}$) bacteria (Fig. 2H). This suggested that the effect of autophagy on SCV maturation/T2-induction is functionally distinct and can be studied specifically using the T2-*gfp* reporter assay.

## Interdependence of autophagy and endosome-to-SCV maturation

To assess the interplay between autophagy, the endosome system and T2 induction, we infected *atg5*$^{-/-}$ and *atg5*$^{+/+}$ MEF expressing markers for early- (Rab5-RFP) or late endosomes (Rab7-RFP) or for lysosomes (Lamp1-RFP) for 2h or 4h with *S*.Tm$^{SopE}$. While *atg5*$^{-/-}$ cells harbored reduced numbers of T2-*gfp* expressing *S*.Tm$^{SopE}$ (Fig. 2A, data not shown), the Rab5- and Lamp1 association with the remaining T2-*gfp* expressing bacteria did not differ in *atg5*$^{-/-}$ vs. *atg5*$^{+/+}$ MEF ($p \geq 0.05$; Fig. 3A,C). Similar observations were made with respect to Rab7, except for a slight difference at 4h p.i. (Fig. 3B). Finally, bafilomycin-mediated inhibition of endosome acidification reduced T2-*gfp* induction in both, *atg5*$^{-/-}$ vs. *atg5*$^{+/+}$ MEF by >10-fold (Fig. S3A). Overall, these data suggest that *atg5*-dependent and *atg5*-independent SCV maturation proceed along similar pathways.

Effects on SCV egress and cytosolic proliferation were assessed by quantifying Rab5, Rab7 and Lamp1 association with "all" *S*.Tm (carrying a constitutive reporter). As expected when most bacteria lodge in intact SCV, the *atg5*$^{+/+}$ data for "all" *S*.Tm was quite similar to that obtained for T2-*gfp*$^{+}$ expressing *S*.Tm (compare Fig. 3A-C to D-F). In *atg5*$^{-/-}$ cells, "all" *S*.Tm showed reduced Rab7 and Lamp1 association by 4h p.i.. This is consistent with SCV escape and cytoplasmic hyper-proliferation. Interestingly, the Rab7- and Lamp1-association was already reduced by 2h p.i. (Fig. 3E,F), a time point preceding the cytoplasmic hyper-proliferation (Fig. 2F-G; Fig. S2J,K). Thus, SCV-egress might occur already by 2h p.i. in *atg5*$^{-/-}$ cells and cytoplasmic bacteria might undergo a lag-phase of 1-2h before hyper-replication commences.

To test the effect of SCV maturation-defects on egress, we infected *atg5*$^{-/-}$ and *atg5*$^{+/+}$ MEF expressing wt, constitutively active (CA) or dominant negative (DN) Rab7-GFP mutants. As expected, (Harrison et al., 2004), the DN Rab7 failed to co-localize with bacteria in wt and mutant MEF (Fig. S3B). In contrast, CA Rab7 was recruited to "all" *S*.Tm with a higher efficiency than wt Rab7. However, even CA Rab7 was recruited with reduced efficiency in *atg5*$^{-/-}$ MEF. Thus, Rab7 activation is needed to recruit Rab7 to the SCV, but Rab7 activation cannot bypass the SCV maturation defect of *atg5*$^{-/-}$ cells.

Finally, we analyzed if Rab5-knockdown affects LC3-association with intracellular *S*.Tm. Supported by previous findings (Smith et al., 2007), combinatorial Rab5A/B/C knockdown reduced T2-*gfp* induction (Fig. S3C). Moreover, the knockdown had minor effects at best on the LC3-recruitment to "all" *S*.Tm (Fig. S3D). Thus, Rab5A/B/C contributes to the initial stages of SCV maturation, but seems dispensable for LC3-recruitment to leaky SCV and/or cytoplasmic *S*.Tm.

## T2-function is dispensable for induction of the T2-*gfp* reporter

T2 is well known to manipulate host-cellular vesicle traffic (Figueira and Holden, 2012). To test if this activity contributes to T2-*gfp* induction, we infected *atg5*$^{-/-}$ and *atg5*$^{+/+}$ MEF with *S*.Tm$^{\Delta T2}$ (SL1344 *sseD::aphT*). T2-*gfp* induction kinetics did not differ significantly between *S*.Tm$^{\Delta T2}$, *S*.Tm$^{SopE}$ and wt *S*.Tm (Fig. 4; compare to Fig. 2E, Fig. S2G). Thus, a functional T2 system does not further promote T2 induction. Much rather, T2 appears to be induced by environmental cues (i.e. vacuolar acidification; Fig. S3A) emanating from the host-cellular endosome-to-SCV maturation process, at least during the first 6h of infection, in murine fibroblasts.

## In the absence of T1, *atg5* is dispensable for T2 induction

So far, it had remained unclear why autophagy promotes T2 expression. T1 can elicit SCV damage, transiently induce autophagy (by ≈1h p.i.) and initiate the restriction of cytosol-exposed *S*.Tm (Birmingham et al., 2006; Ivanov and Roy, 2009; Tattoli et al., 2012). To test if the autophagy-promoted T2-induction roots in T1-inflicted membrane damage, *atg5*$^{-/-}$ and *atg5*$^{+/+}$ MEF were infected with *S*.Tm$^{\Delta T1}$ (SL1344, Δ*invG*; T1 defective; Table S1A). *S*.Tm$^{\Delta T1}$ internalization was promoted by co-infection with *S*.Tm$^{SopE}$ (=helper, 1:5 mixture with *S*.Tm$^{\Delta T1}$pT2-*gfp*; (Birmingham et al., 2006; Misselwitz et al., 2011a; Steele-Mortimer et al., 2002)). Lamp1 staining suggested that *S*.Tm$^{\Delta T1}$ and *S*.Tm$^{SopE}$ do generally reside in separate SCVs (Fig. S4A-C). Intriguingly, the time course of T2-*gfp* expression by *S*.Tm$^{\Delta T1}$ (Fig. 5A) was similar to that of *S*.Tm$^{SopE}$ (Fig. 2E), but did not differ between *atg5*$^{-/-}$ and *atg5*$^{+/+}$ cells ($p \geq 0.05$). Moreover, plating indicated that *S*.Tm$^{\Delta T1}$ did not grow intracellularly, neither in *atg5*$^{-/-}$ nor in *atg5*$^{+/+}$ cells for 6h p.i. ($p \geq 0.05$; Fig. 5B,C). This suggested that, even in the absence of autophagy, *S*.Tm$^{\Delta T1}$ remained in a vacuolar compartment and therefore did not engage in cytosolic hyper-replication (Fig. S2C,D). Equivalent data were obtained when internalization of *S*.Tm$^{\Delta T1}$ was driven by a plasmid expressing Invasin (Fig. S4D-F), a well-characterized adhesin from *Yersinia pseudotuberculosis* (Hardt et al., 1998; Isberg and Van Nhieu, 1995; Isberg et al., 1987). Taken together, these data imply that T1-inflicted SCV damage elicits not only the tagging and elimination of cytosol-exposed bacteria

(Braun et al., 2010; Malik-Kale et al., 2012; Mallo et al., 2008), but also the sealing of the damaged SCV which promotes T2-induction.

## LC3 is recruited in a T1-dependent fashion

To establish the kinetics of T1-mediated autophagy-induction, we analyzed the time course of LC3 recruitment. LC3 is recruited and conjugated in an ATG5-dependent fashion to *S*.Tm lodged in ruptured endosomes or the host cell cytosol (Birmingham et al., 2006; Fujita et al., 2008; Hanada et al., 2007). In *S*.Tm$^{SopE}$-infected wt (but not *atg5*$^{-/-}$) MEF, LC3 was recruited as early as 40 min p.i., peaked at 40-60 min and declined by 90-240 min p.i. (Fig. 6A,B). In contrast, "helped" invasion of *S*.Tm$^{\Delta T1}$ (helper = *S*.Tm$^{SopE}$) did not yield any LC3-recruitment, neither in the *atg5*$^{-/-}$ nor the *atg5*$^{+/+}$ cells (Fig. S5A,B). These data verified that autophagy is activated already at early stages after invasion by T1-positive bacteria, while T1-deficient bacteria do not activate this host-cellular response.

Interestingly, some internalized *S*.Tm$^{SopE}$ cells acquired LC3, while others did not (Fig. 6A). We speculated that this is attributable to the "bimodal" T1 expression of *S*.Tm (Hautefort et al., 2003; Saini et al., 2010; Schlumberger et al., 2005; Sturm et al., 2011; Winnen et al., 2008). Thereby, the inoculum of wt *S*.Tm or *S*.Tm$^{SopE}$ harbors about 30% of T1-expressing cells (T1-"on") and 70% T1-"off" cells. Only the T1-on bacteria trigger membrane ruffles (and inflict T1 damage; should lead to transient LC3 recruitment and repair or to egress), while T1-off bacteria enter passively (i.e. like *S*.Tm$^{\Delta T1}$ in Fig. 5). When we infected *atg5*$^{+/+}$ cells (*atg5*$^{-/-}$ = neg. control) for 40 min with *S*.Tm$^{SopE}$, the LC3 recruitment to the average invading bacterium was significantly higher at MOI = 1 than at MOI = 10 ($p < 0.05$; Fig. 6C). Similarly, in infections with *S*.Tm$^{SopE}$ (T2-*gfp* reporter, MOI=1) the LC3 recruitment to the bacteria was strikingly similar between T2-*gfp*$^{+}$ and "all" bacteria (constitutive reporter; $p > 0.05$; Fig. 6D). Similar observations were made with recruitment of Galectin-3, a cytosolic "danger receptor" (Fig. S5C-E). These data provided further support that T1-inflicts endosome damage and that autophagy promotes its repair thereby fostering endosome-to-SCV maturation and T2-induction.

## Fluid-phase marker retention confirmed the role of autophagy in SCV repair

To verify delayed endosome repair in the autophagy-deficient cells, *atg5*$^{-/-}$ and *atg5*$^{+/+}$ MEF were incubated with FITC-dextran (500kDa) and infected for 90 min with *S*.Tm$^{SopE}$. FITC-dextran retention in SCVs was more pronounced in *atg5*$^{+/+}$ than in *atg5*$^{-/-}$ cells ($p < 0.05$; Fig. 7A). No such difference was observed in *S*.Tm$^{\Delta T1}$ infections ($p \geq 0.05$; helper=*S*.Tm$^{SopE}$). We also quantified FITC-dextran retention in SCVs showing evidence of membrane damage. Galectin-3-mOrange expressing *atg5*$^{-/-}$ and *atg5*$^{+/+}$ MEF were infected for 90 min with *S*.Tm$^{SopE}$. Galectin-3-positive SCVs yielded lower FITC-dextran

signals than the average SCV, both, in the *atg5*$^{-/-}$ and the *atg5*$^{+/+}$ cells (Fig. 7A). This confirmed that T1-compromises SCV-integrity and that autophagy supports the sealing of damaged SCV membranes.

Finally, we analyzed the effect of osmotic shock-inflicted membrane damage. *Atg5*$^{-/-}$ and *atg5*$^{+/+}$ MEF expressing Galectin-3-mOrange were treated with Blue-dextran (500kDa) and HGF to allow internalization of *S*.Tm$^{\Delta T1}$ (constitutive *gfp*). We inflicted membrane damage (10 min, 0.5M sucrose + 10% PEG1000 followed by 3min in 60%PBS) and analyzed dye-dextran retention in the vicinity of *gfp*-expressing bacteria. Osmotic shock slightly reduced dye-dextran retention in *atg5*$^{+/+}$ controls (Fig. 7B,C). More pronounced loss of dye-dextran retention was observed in *atg5*$^{-/-}$ cells. This may suggest a general role for autophagy in maintaining endosome membrane integrity.

# Discussion

Our study identified a novel function of autophagy during repair of T1-inflicted SCV damage at the early stages of *S*.Tm infection. This fosters SCV maturation and thereby promotes T2-induction (see working model; Fig. 7D), which is distinct from the well-described function of autophagy in tagging ruptured endosomes and lysosomal killing of cytosolic *S*.Tm (Birmingham et al., 2006; Tattoli et al., 2012; Thurston et al., 2012). Thus, autophagy controls two different effector mechanisms during infection. Both mechanisms are needed to confine the majority of the invading *S*.Tm cells to the SCV and thereby promote T2 expression by the vast majority of internalized bacteria.

SCV-membrane sealing seem to require regulators (mTOR), recruitment factors (galectins, Optineurin), initiation factors (ULK1, PI3-kinase C3, Beclin-1, ATG2A, ATG9) as well as the ATG12- (ATG5, ATG7, ATG12, ATG16L1) and ATG8-conjugation systems. Individual elements (MAP1LC3A, MAP1LC3B, MAP1LC3C, GABARAPL1, GABARAPL2, and GABARAP) of the ATG8-conjugation system had only mild effects at best, which is likely attributable to functional redundancy. LC3 recruitment to *S*.Tm is thought to occur through the canonical autophagy pathway involving ULK1, Beclin1 and ATG9 or through LC3-associated phagocytosis (LAP), requiring diacylglycerol (Shahnazari et al., 2010) and protein kinase Cδ (PKCδ)-mediated activation of NADPH oxidase and reactive oxygen species (ROS) (Fontayne et al., 2002; Huang et al., 2009). Autophagy-dependent SCV repair required ULK1, Beclin1 and ATG9 (Fig. 1), suggesting that LC3 is recruited to the damaged SCV by canonical autophagy, not by LAP.

Three lines of evidence exclude that cytoplasmic hyper-replication in autophagy-deficient cells affects our assessment of T2-expression by SCV-lodged bacteria. i) The diminished T2-induction was concurrent with the onset of the T2-*gfp* reporter expression (Fig. 2E; 1-3h p.i), ii) this preceded the onset of cytosolic *S*.Tm growth, which became apparent only much later (4-6h p.i.; Fig. 2F) and iii) the T2-*gfp* expression kinetics by *S*.Tm$^{\Delta T1}$ (which remains in the SCV even in *atg5*$^{-/-}$ cells) were not affected

by the cytoplasmic hyper-proliferation of the reporter-less "helper" strain *S*.Tm$^{SopE}$ (Fig. 5C). Thus, both autophagy-dependent effector mechanisms can operate "in parallel" and cytoplasmic hyper-replication does not interfere with the membrane sealing and T2 expression by SCV-lodged *S*.Tm.

It is interesting to note that T1 is not only driving invasion of epithelial cells and fibroblasts, but also the prime cause for endosomal membrane damage. Thus, the T1-expressing bacteria rely on a host cellular system (i.e. autophagy), to initiate repair of this membrane damage before the SCV can mature further, acidify and allow the expression of T2. Strikingly, the T1-deficient bacteria (invading by helper-triggered ruffling or by Invasin expression) can bypass this need for autophagy as they do not cause endosome membrane damage. This latter phenomenon may be of relevance for the wt *S*.Tm infection, as wt *S*.Tm forms 30% T1-expressing- and 70% non-expressing bacterial cells (Ackermann et al., 2008; Diard et al., 2013; Hautefort et al., 2003; Schlumberger et al., 2005; Sturm et al., 2011). The T1-on bacteria require autophagy-promoted SCV repair, while the T1-off bacteria are entering by "helped" invasion, do not compromise SCV integrity and thus bypass this need for autophagy. This is a striking example of an intricate pathogen-host interaction whereby the pathogen (i.e. the T1-on bacteria) relies on specific host responses in order to maintain an intracellular niche and coordinate virulence factor expression.

The cellular processes sealing the damaged SCV membrane remain to be established. Clearly, the ATG12-conjugation system is involved and thereby promotes SCV maturation, vacuolar acidification, T2 expression and the secretion of SPI-2 effectors to facilitate downstream events of the infection process. In the absence of functional autophagy, the dynamics of SCV repair are impaired and stall the compromised SCVs in a Rab5-positive stage, which is prone to bacterial egress and subsequent hyper-proliferation at cytosolic sites later during infection.

Some evidence suggests that autophagy is of relevance for the infection *in vivo*. Enterocyte-specific ablation of *atg5*, *atg16L1* or *atg7* in mice affected mucosal inflammatory responses and rendered the animals prone to systemic pathogen dissemination by *S*.Tm (Benjamin et al., 2013; Conway et al., 2013) and other enteric pathogens (Marchiando et al., 2013). However, the exact role of autophagy and the relative contribution of SCV-repair, cytoplasmic pathogen elimination or undiscovered effector functions remains to be established. One might speculate if some *Salmonella* strains may express virulence factors manipulating such responses. Up to date, RavZ from *Legionella pneumophila* is the only bacterial effector known to manipulate autophagy, i.e. by irreversibly deconjugating LC3 from the surface of pre-autophagosomal membranes (Amer and Swanson, 2005; Choy et al., 2012).

In the past years, there is accumulating evidence suggesting that autophagy can affect pathogen traffic in different ways. In case of *Brucella abortus*, the pathogen-containing vacuole matures into a reticulum-like compartment (BCV) fostering pathogen replication. In this case, pathogen release from the infected cell requires the recruitment of autophagy initiation factors like ULK1 and Beclin1 to the

BCV, while autophagy-elongation proteins (e.g. ATG5, ATG16L1, ATG4B, ATG7, and LC3B) were not needed (Starr et al., 2012). By contrast, the *Coxiella*-containing vacuole is decorated with LC3 throughout all intracellular phases of the infection which is thought to delay the fusion with lysosomes (Beron et al., 2002; Gutierrez et al., 2005; Romano et al., 2007). These cases are yet clearly different from the role of autophagy in *S*.Tm infection. Our findings of autophagy-dependent repair of SCVs harboring the T1-expressing *Salmonella* population in infected cells extend the mechanisms that are subverted by bacterial pathogens and emphasize the central role of autophagy in the pathogen-host cell interaction.

It has become clear that autophagy not only affects the handling of intracellular pathogens, but also "sterile" endosomes not harboring any bacteria (Thurston et al., 2012). In fact, endosome membrane defects in non-infected cells are efficiently tagged by Galectin-3, -8 and -9 (but not by Galectin-1, (Thurston et al., 2012)). Our osmotic-shock data (Fig. 7B,C) suggest that this might initiate endosome membrane repair. It will be interesting to find out if autophagy-mediated endosome membrane repair is of general importance for maintaining the endosomal membrane integrity in mammalian cells.

**Author contributions:** S.K. and W.D.H. designed the experiments; S.K. performed the experiments; J.F. performed EM; M.E. and P.R. analyzed screening data; M.E, P.R. and C.D. contributed to data analysis; J.F. and J.E. provided Galectin-3 constructs and supported design of experiments, C.M. provided ATG5-deficient murine fibroblasts and helped throughout discussions, and S.K and W.D.H wrote the manuscript.

**Acknowledgements**

We thank F. Randow, D. Holden, M. Sellin, Hardt lab members and the members of InfectX/TargetInfectX and ScopeM, i.e. F. Schmich, D. Andritschke and J. Mercer (also for marker constructs), for help with the GWS and in depth discussions. M. Sachse, J. Krijnse-Locker (Institut Pasteur Ultrapole) and A. Weiner provided invaluable help with correlative EM. The work was funded by SystemsX.ch, the Swiss Initiative in Systems Biology, RTD grants 51RT-0_126008 (InfectX) and 51RTP0_151029 (TargetInfectX), evaluated by the Swiss National Science Foundation and Swiss National Science Foundation grant 310030_153074/1 to WDH. Further support was received from SyBIT, the IT project of SystemsX. JE is member of the LabEx consortium IBEID, and is supported by the Institut Pasteur CARNOT-MIE programme and an ERC starting grant (Rupteffects, Nr. 261166). JF was supported a Pasteur Foundation fellowship.

# Experimental Procedures

**Cells and plasmids**

Wt *S*.Tm (SL1344), *S*.Tm$^{SopE}$ (SL1344, *sopE2sipAsopE*), *S*.Tm$^{\Delta T1}$ (SL1344, *invG*), *S*.Tm$^{\Delta T2}$ (SL1344, *sseD*), HeLa CCL-2 cells, *atg5*$^{+/+}$ and *atg5*$^{-/-}$ mouse embryonic fibroblasts, the plasmids pM965, pM975 and pWRG435 and the expression constructs for wt and mutant forms of Rab5A, Rab7, Lamp1, Galectin-3, lentiviral transduction and transient transfection are described in the Supplement. Bacteria were grown under T1-inducing conditions in LB (0.3M NaCl) as described (Misselwitz et al., 2011a).

**siRNA screen**

Cell culture in 96 or 384-well format, reverse RNA transfection, controls, infection, staining, automated imaging and automated image analysis were performed in HeLa CCL-2 using the InfectX pipeline as described in the Supplement. RNA libraries included the Dharmacon ONTARGETplus SMART pool Library (18.237 genes), customized siRNA libraries (Ambion Silencer and Silencer Select; esiRNAs (Sigma)) and kinome-targeting siRNAs (see Supplement, Table S1B). The pathogen-specific control siRNAs present in every screening plate were ArpC3, Cdc42, ATP6V1A (reduced infection) and ITGAV and CFL1 (enhanced infection) (Misselwitz et al., 2011a). Cells were infected for 20min with *S*.Tm$^{SopE}$ harboring pM975 (T2-*gfp* reporter; MOI=80), incubated 3h 40min in medium with 400µg/ml gentamicin, fixed (4% PFA, 4% sucrose) and stained with DAPI and DY-547-phalloidin. All liquid handling steps (infection, fixation and staining) were performed with a liquid handling robot (BioTek; EL406). After high-throughput image acquisition of the 384-well screening plates using the Molecular Devices ImageXpress microscope (10X S Fluor; 1000-3500 cells per well), a CellProfiler-based image analysis pipeline was applied. The analysis involved shading correction to compensate for uneven microscope-based illumination and detected SCV-residing *S*.Tm through a wavelet-based small particle detector CellProfiler module. Herewith, we extracted on average 550 features for five distinct objects (bacteria, nuclei, cells, perinuclei and voronoi cells) out of 1.8 million images and in total more than 100 million cells.

**Step-specific assays**

Assays were performed as described ((Misselwitz et al., 2011b) for details, see Supplement). Binding to MEF was analyzed by 6min *S*.Tm$^{\Delta 4}$ infection (MOI=125), washing and automated microscopy quantification of surface-attached bacteria. Ruffling was quantified after 12min *S*.Tm$^{SopE}$ (pM965; MOI=80) infection, phalloidin staining, Z-stack imaging and blinded quantification of membrane ruffles. The classical gentamicin-protection assay was performed in 20min infections (MOI=10), subsequent incubation in gentamicin-medium for the indicated times and plating-enumeration of the remaining intracellular bacteria. For helper assays and invasion-mediated invasion, higher MOI were applied (see Supplement).

**Statistics**

The number of biological replicates was sufficient to perform statistics using the non-parametric Mann-Whitney U test, comparing individual data points for experimental- and control samples.

**Fluorescence microcopy and quantitative analysis of co-localization**

Cells transfected or dye-dextran-loaded (FITC-dextran, 500kDa; Blue-dextran, 500kDa) were infected as indicated, and exposed to osmotic shock (as indicated), fixed and stained, imaged with a 100x-objective, a spinning disc head and a Zeiss Axiovert 200m microscope and marker co-localization was analyzed with Volocity (quantitation module) as detailed in the Supplement.

# References


Ackermann, M., B. Stecher, N.E. Freed, P. Songhet, W.D. Hardt, and M. Doebeli. 2008. Self-destructive cooperation mediated by phenotypic noise. *Nature* 454:987-990.

Amer, A.O., and M.S. Swanson. 2005. Autophagy is an immediate macrophage response to Legionella pneumophila. *Cellular microbiology* 7:765-778.

Bakowski, M.A., V. Braun, and J.H. Brumell. 2008. Salmonella-containing vacuoles: directing traffic and nesting to grow. *Traffic* 9:2022-2031.

Baxt, L.A., A.C. Garza-Mayers, and M.B. Goldberg. 2013. Bacterial subversion of host innate immune pathways. *Science* 340:697-701.

Benjamin, J.L., R. Sumpter, Jr., B. Levine, and L.V. Hooper. 2013. Intestinal epithelial autophagy is essential for host defense against invasive bacteria. *Cell host & microbe* 13:723-734.

Beron, W., M.G. Gutierrez, M. Rabinovitch, and M.I. Colombo. 2002. Coxiella burnetii localizes in a Rab7-labeled compartment with autophagic characteristics. *Infection and immunity* 70:5816-5821.

Birmingham, C.L., A.C. Smith, M.A. Bakowski, T. Yoshimori, and J.H. Brumell. 2006. Autophagy controls Salmonella infection in response to damage to the Salmonella-containing vacuole. *The Journal of biological chemistry* 281:11374-11383.

Braun, V., A. Wong, M. Landekic, W.J. Hong, S. Grinstein, and J.H. Brumell. 2010. Sorting nexin 3 (SNX3) is a component of a tubular endosomal network induced by Salmonella and involved in maturation of the Salmonella-containing vacuole. *Cellular microbiology* 12:1352-1367.

Brumell, J.H., P. Tang, M.L. Zaharik, and B.B. Finlay. 2002. Disruption of the Salmonella-containing vacuole leads to increased replication of Salmonella enterica serovar typhimurium in the cytosol of epithelial cells. *Infection and immunity* 70:3264-3270.

Choy, A., J. Dancourt, B. Mugo, T.J. O'Connor, R.R. Isberg, T.J. Melia, and C.R. Roy. 2012. The Legionella effector RavZ inhibits host autophagy through irreversible Atg8 deconjugation. *Science* 338:1072-1076.

Conway, K.L., P. Kuballa, J.H. Song, K.K. Patel, A.B. Castoreno, O.H. Yilmaz, H.B. Jijon, M. Zhang, L.N. Aldrich, E.J. Villablanca, J.M. Peloquin, G. Goel, I.A. Lee, E. Mizoguchi, H.N. Shi, A.K. Bhan, S.Y. Shaw, S.L. Schreiber, H.W. Virgin, A.F. Shamji, T.S. Stappenbeck, H.C. Reinecker, and R.J. Xavier. 2013. Atg16l1 is Required for Autophagy in Intestinal Epithelial Cells and Protection of Mice From Salmonella Infection. *Gastroenterology* 145:1347-1357.

Diard, M., V. Garcia, L. Maier, M.N. Remus-Emsermann, R.R. Regoes, M. Ackermann, and W.D. Hardt. 2013. Stabilization of cooperative virulence by the expression of an avirulent phenotype. *Nature* 494:353-356.

Figueira, R., and D.W. Holden. 2012. Functions of the Salmonella pathogenicity island 2 (SPI-2) type III secretion system effectors. *Microbiology* 158:1147-1161.

Fontayne, A., P.M. Dang, M.A. Gougerot-Pocidalo, and J. El-Benna. 2002. Phosphorylation of p47phox sites by PKC alpha, beta II, delta, and zeta: effect on binding to p22phox and on NADPH oxidase activation. *Biochemistry* 41:7743-7750.

Franceschini, A., R. Meier, A. Casanova, S. Kreibich, N. Daga, D. Andritschke, S. Dilling, P. Ramo, M. Emmenlauer, A. Kaufmann, R. Conde-Alvarez, S.H. Low, L. Pelkmans, A. Helenius, W.D. Hardt, C. Dehio, and C. von Mering. 2014. Specific inhibition of diverse pathogens in human cells by synthetic microRNA-like oligonucleotides inferred from RNAi screens. *Proceedings of the National Academy of Sciences of the United States of America* 111:4548-4553.

Fredlund, J., and J. Enninga. 2014. Cytoplasmic access by intracellular bacterial pathogens. *Trends in microbiology* 22:128-137.

Fujita, N., T. Itoh, H. Omori, M. Fukuda, T. Noda, and T. Yoshimori. 2008. The Atg16L complex specifies the site of LC3 lipidation for membrane biogenesis in autophagy. *Molecular biology of the cell* 19:2092-2100.

Gutierrez, M.G., C.L. Vazquez, D.B. Munafo, F.C. Zoppino, W. Beron, M. Rabinovitch, and M.I. Colombo. 2005. Autophagy induction favours the generation and maturation of the Coxiella-replicative vacuoles. *Cellular microbiology* 7:981-993.

Hanada, T., N.N. Noda, Y. Satomi, Y. Ichimura, Y. Fujioka, T. Takao, F. Inagaki, and Y. Ohsumi. 2007. The Atg12-Atg5 conjugate has a novel E3-like activity for protein lipidation in autophagy. *The Journal of biological chemistry* 282:37298-37302.

Hardt, W.D., L.M. Chen, K.E. Schuebel, X.R. Bustelo, and J.E. Galan. 1998. S. typhimurium encodes an activator of Rho GTPases that induces membrane ruffling and nuclear responses in host cells. *Cell* 93:815-826.

Harrison, R.E., J.H. Brumell, A. Khandani, C. Bucci, C.C. Scott, X. Jiang, B.B. Finlay, and S. Grinstein. 2004. Salmonella impairs RILP recruitment to Rab7 during maturation of invasion vacuoles. *Molecular biology of the cell* 15:3146-3154.

Hautefort, I., M.J. Proenca, and J.C. Hinton. 2003. Single-copy green fluorescent protein gene fusions allow accurate measurement of Salmonella gene expression in vitro and during infection of mammalian cells. *Applied and environmental microbiology* 69:7480-7491.

Huang, J., and J.H. Brumell. 2014. Bacteria-autophagy interplay: a battle for survival. *Nature reviews. Microbiology* 12:101-114.

Huang, J., V. Canadien, G.Y. Lam, B.E. Steinberg, M.C. Dinauer, M.A. Magalhaes, M. Glogauer, S. Grinstein, and J.H. Brumell. 2009. Activation of antibacterial autophagy by NADPH oxidases. *Proceedings of the National Academy of Sciences of the United States of America* 106:6226-6231.

Isberg, R.R., and G.T. Van Nhieu. 1995. The mechanism of phagocytic uptake promoted by invasin-integrin interaction. *Trends in cell biology* 5:120-124.

Isberg, R.R., D.L. Voorhis, and S. Falkow. 1987. Identification of invasin: a protein that allows enteric bacteria to penetrate cultured mammalian cells. *Cell* 50:769-778.

Ivanov, S., and C.R. Roy. 2009. NDP52: the missing link between ubiquitinated bacteria and autophagy. *Nature immunology* 10:1137-1139.

Kaiser, P., M. Diard, B. Stecher, and W.D. Hardt. 2012. The streptomycin mouse model for Salmonella diarrhea: functional analysis of the microbiota, the pathogen's virulence factors, and the host's mucosal immune response. *Immunological reviews* 245:56-83.

Knodler, L.A., V. Nair, and O. Steele-Mortimer. 2014. Quantitative assessment of cytosolic salmonella in epithelial cells. *PloS one* 9:e84681.

Knodler, L.A., B.A. Vallance, J. Celli, S. Winfree, B. Hansen, M. Montero, and O. Steele-Mortimer. 2010. Dissemination of invasive Salmonella via bacterial-induced extrusion of mucosal epithelia. *Proceedings of the National Academy of Sciences of the United States of America* 107:17733-17738.

Kuballa, P., A. Huett, J.D. Rioux, M.J. Daly, and R.J. Xavier. 2008. Impaired autophagy of an intracellular pathogen induced by a Crohn's disease associated ATG16L1 variant. *PloS one* 3:e3391.

Kuma, A., M. Hatano, M. Matsui, A. Yamamoto, H. Nakaya, T. Yoshimori, Y. Ohsumi, T. Tokuhisa, and N. Mizushima. 2004. The role of autophagy during the early neonatal starvation period. *Nature* 432:1032-1036.

Levine, B., N. Mizushima, and H.W. Virgin. 2011. Autophagy in immunity and inflammation. *Nature* 469:323-335.

Luo, W., and C. Brouwer. 2013. Pathview: an R/Bioconductor package for pathway-based data integration and visualization. *Bioinformatics* 29:1830-1831.

Malik-Kale, P., S. Winfree, and O. Steele-Mortimer. 2012. The bimodal lifestyle of intracellular Salmonella in epithelial cells: replication in the cytosol obscures defects in vacuolar replication. *PloS one* 7:e38732.

Mallo, G.V., M. Espina, A.C. Smith, M.R. Terebiznik, A. Aleman, B.B. Finlay, L.E. Rameh, S. Grinstein, and J.H. Brumell. 2008. SopB promotes phosphatidylinositol 3-phosphate formation on Salmonella vacuoles by recruiting Rab5 and Vps34. *The Journal of cell biology* 182:741-752.

Marchiando, A.M., D. Ramanan, Y. Ding, L.E. Gomez, V.M. Hubbard-Lucey, K. Maurer, C. Wang, J.W. Ziel, N. van Rooijen, G. Nunez, B.B. Finlay, I.U. Mysorekar, and K. Cadwell. 2013. A deficiency in the autophagy gene Atg16L1 enhances resistance to enteric bacterial infection. *Cell host & microbe* 14:216-224.

Misselwitz, B., S. Dilling, P. Vonaesch, R. Sacher, B. Snijder, M. Schlumberger, S. Rout, M. Stark, C. von Mering, L. Pelkmans, and W.D. Hardt. 2011a. RNAi screen of Salmonella invasion shows role of COPI in membrane targeting of cholesterol and Cdc42. *Molecular systems biology* 7:474.

Misselwitz, B., S.K. Kreibich, S. Rout, B. Stecher, B. Periaswamy, and W.D. Hardt. 2011b. Salmonella enterica serovar Typhimurium binds to HeLa cells via Fim-mediated reversible adhesion and irreversible type three secretion system 1-mediated docking. *Infection and immunity* 79:330-341.

Mizushima, N., A. Kuma, Y. Kobayashi, A. Yamamoto, M. Matsubae, T. Takao, T. Natsume, Y. Ohsumi, and T. Yoshimori. 2003. Mouse Apg16L, a novel WD-repeat protein, targets to the autophagic isolation membrane with the Apg12-Apg5 conjugate. *Journal of cell science* 116:1679-1688.

Mizushima, N., A. Yamamoto, M. Hatano, Y. Kobayashi, Y. Kabeya, K. Suzuki, T. Tokuhisa, Y. Ohsumi, and T. Yoshimori. 2001. Dissection of autophagosome formation using Apg5-deficient mouse embryonic stem cells. *The Journal of cell biology* 152:657-668.

Nakagawa, I., A. Amano, N. Mizushima, A. Yamamoto, H. Yamaguchi, T. Kamimoto, A. Nara, J. Funao, M. Nakata, K. Tsuda, S. Hamada, and T. Yoshimori. 2004. Autophagy defends cells against invading group A Streptococcus. *Science* 306:1037-1040.

Ogawa, M., T. Yoshimori, T. Suzuki, H. Sagara, N. Mizushima, and C. Sasakawa. 2005. Escape of intracellular Shigella from autophagy. *Science* 307:727-731.

Rathman, M., M.D. Sjaastad, and S. Falkow. 1996. Acidification of phagosomes containing Salmonella typhimurium in murine macrophages. *Infection and immunity* 64:2765-2773.

Romano, P.S., M.G. Gutierrez, W. Beron, M. Rabinovitch, and M.I. Colombo. 2007. The autophagic pathway is actively modulated by phase II Coxiella burnetii to efficiently replicate in the host cell. *Cellular microbiology* 9:891-909.

Saini, S., J.R. Ellermeier, J.M. Slauch, and C.V. Rao. 2010. Correction: The role of coupled positive feedback in the expression of the SPI1 type three secretion system in Salmonella. *PLoS pathogens* 6:

Schlumberger, M.C., and W.D. Hardt. 2006. Salmonella type III secretion effectors: pulling the host cell's strings. *Current opinion in microbiology* 9:46-54.

Schlumberger, M.C., R. Kappeli, M. Wetter, A.J. Muller, B. Misselwitz, S. Dilling, M. Kremer, and W.D. Hardt. 2007. Two newly identified SipA domains (F1, F2) steer effector protein localization and contribute to Salmonella host cell manipulation. *Molecular microbiology* 65:741-760.

Schlumberger, M.C., A.J. Muller, K. Ehrbar, B. Winnen, I. Duss, B. Stecher, and W.D. Hardt. 2005. Real-time imaging of type III secretion: Salmonella SipA injection into host cells. *Proceedings of the National Academy of Sciences of the United States of America* 102:12548-12553.

Shahnazari, S., A. Namolovan, D.J. Klionsky, and J.H. Brumell. 2011. A role for diacylglycerol in antibacterial autophagy. *Autophagy* 7:331-333.

Shahnazari, S., W.L. Yen, C.L. Birmingham, J. Shiu, A. Namolovan, Y.T. Zheng, K. Nakayama, D.J. Klionsky, and J.H. Brumell. 2010. A diacylglycerol-dependent signaling pathway contributes to regulation of antibacterial autophagy. *Cell host & microbe* 8:137-146.

Smith, A.C., J.T. Cirulis, J.E. Casanova, M.A. Scidmore, and J.H. Brumell. 2005. Interaction of the Salmonella-containing vacuole with the endocytic recycling system. *The Journal of biological chemistry* 280:24634-24641.

Smith, A.C., W.D. Heo, V. Braun, X. Jiang, C. Macrae, J.E. Casanova, M.A. Scidmore, S. Grinstein, T. Meyer, and J.H. Brumell. 2007. A network of Rab GTPases controls phagosome maturation and is modulated by Salmonella enterica serovar Typhimurium. *The Journal of cell biology* 176:263-268.

Starr, T., R. Child, T.D. Wehrly, B. Hansen, S. Hwang, C. Lopez-Otin, H.W. Virgin, and J. Celli. 2012. Selective subversion of autophagy complexes facilitates completion of the Brucella intracellular cycle. *Cell host & microbe* 11:33-45.

Steele-Mortimer, O., J.H. Brumell, L.A. Knodler, S. Meresse, A. Lopez, and B.B. Finlay. 2002. The invasion-associated type III secretion system of Salmonella enterica serovar Typhimurium is necessary for intracellular proliferation and vacuole biogenesis in epithelial cells. *Cellular microbiology* 4:43-54.

Sturm, A., M. Heinemann, M. Arnoldini, A. Benecke, M. Ackermann, M. Benz, J. Dormann, and W.D. Hardt. 2011. The cost of virulence: retarded growth of Salmonella Typhimurium cells expressing type III secretion system 1. *PLoS pathogens* 7:e1002143.

Tattoli, I., M.T. Sorbara, D. Vuckovic, A. Ling, F. Soares, L.A. Carneiro, C. Yang, A. Emili, D.J. Philpott, and S.E. Girardin. 2012. Amino acid starvation induced by invasive bacterial pathogens triggers an innate host defense program. *Cell host & microbe* 11:563-575.

Thurston, T.L., G. Ryzhakov, S. Bloor, N. von Muhlinen, and F. Randow. 2009. The TBK1 adaptor and autophagy receptor NDP52 restricts the proliferation of ubiquitin-coated bacteria. *Nature immunology* 10:1215-1221.

Thurston, T.L., M.P. Wandel, N. von Muhlinen, A. Foeglein, and F. Randow. 2012. Galectin 8 targets damaged vesicles for autophagy to defend cells against bacterial invasion. *Nature* 482:414-418.

Watson, R.O., P.S. Manzanillo, and J.S. Cox. 2012. Extracellular M. tuberculosis DNA targets bacteria for autophagy by activating the host DNA-sensing pathway. *Cell* 150:803-815.

Wild, P., H. Farhan, D.G. McEwan, S. Wagner, V.V. Rogov, N.R. Brady, B. Richter, J. Korac, O. Waidmann, C. Choudhary, V. Dotsch, D. Bumann, and I. Dikic. 2011. Phosphorylation of the autophagy receptor optineurin restricts Salmonella growth. *Science* 333:228-233.

Winnen, B., M.C. Schlumberger, A. Sturm, K. Schupbach, S. Siebenmann, P. Jenny, and W.D. Hardt. 2008. Hierarchical effector protein transport by the Salmonella Typhimurium SPI-1 type III secretion system. *PloS one* 3:e2178.

Yoshikawa, Y., M. Ogawa, T. Hain, M. Yoshida, M. Fukumatsu, M. Kim, H. Mimuro, I. Nakagawa, T. Yanagawa, T. Ishii, A. Kakizuka, E. Sztul, T. Chakraborty, and C. Sasakawa. 2009. Listeria monocytogenes ActA-mediated escape from autophagic recognition. *Nature cell biology* 11:1233-1240.

Yu, H.B., M.A. Croxen, A.M. Marchiando, R.B. Ferreira, K. Cadwell, L.J. Foster, and B.B. Finlay. 2014. Autophagy facilitates Salmonella replication in HeLa cells. *mBio* 5:e00865-00814.

Yu, X.J., K. McGourty, M. Liu, K.E. Unsworth, and D.W. Holden. 2010. pH sensing by intracellular Salmonella induces effector translocation. *Science* 328:1040-1043.

Zheng, Y.T., S. Shahnazari, A. Brech, T. Lamark, T. Johansen, and J.H. Brumell. 2009. The adaptor protein p62/SQSTM1 targets invading bacteria to the autophagy pathway. *Journal of immunology* 183:5909-5916.

# Figure Legends

**Figure 1: Genome-wide RNAi screen implicating autophagy**. **A)** T2-*gfp* reporter assay (see Supplement; (Misselwitz et al., 2011b). **B,C)** Image-based screen of HeLa nuclei (DAPI), actin (DY-547 phalloidin) and T2-*gfp*-expression. Bar=10µm. CellProfiler-based identification of nuclei, cell borders and T2-*gfp*-expressing *S*.Tm$^{SopE}$ (Supplement). **D)** Results (data shown in Table S1B). Autophagy was identified by KEGG-pathway analysis (Luo and Brouwer, 2013) and phenotypic clustering of the 5000 strongest hits. Red frames=hits from earlier work (Misselwitz et al., 2011a) and inhibitors. **E-H)** Knockdown phenotypes (z-scores) of autophagy hits from Table S1B. Dots=screen data (black=GWS; grey=Ambion; red=esiRNA; turquoise=Qiagen; dark/light blue=Dharmacon pooled/unpooled); bar=mean with SD. Color code as in D. Stippled line: cutoff=-0.5 z-score (≈30% attenuation). ATG7 is involved in ATG12- and ATG8 systems (G and H).

**Figure 2: Impact of *atg5* on distinct stages of *S*.Tm infection. A)** T2-g*fp* expression at 4h p.i. of *atg5*$^{+/+}$ (dark) or *atg5*$^{-/-}$ (light grey) MEF with *S*.Tm$^{SopE}$ (MOI=60). **B)** Binding of *S*.Tm$^{\Delta 4}$ (MOI=125; 6min p.i.). **C)** Ruffling triggered by *S*.Tm$^{SopE}$ (MOI=80; 12min p.i.; 571 or 549 cells analyzed). **D)** Gentamicin-protection assay (*S*.Tm$^{SopE}$ cfu; 1h p.i.; MOI=10). **E)** Time course of *S*.Tm$^{SopE}$ infection (T2-*gfp* assay (1- 12h p.i.; MOI=40). **F)** Gentamicin-protection time course assay (*S*.Tm$^{SopE}$ cfu; MOI=10). **G)** Intracellular growth ([cfu (6h p.i.)]/[cfu (2h p.i.]); data from F. **H)** Fluorescence microcopy of *atg5*$^{+/+}$ of *atg5*$^{-/-}$ MEF 6h p.i. with *S*.Tm$^{SopE}$. red=α-LPS-CY5 (="all *S*.Tm"); green= T2-g*fp*; blue=DAPI. Bar=5µm. All data were from ≥5 independent replicates (whisker bar=mean and SD).

**Figure 3: Endosome marker localization to *S*.Tm$^{SopE}$ in wt or *atg5*$^{-/-}$ MEF**. MEF transfected with endosome-reporters as indicated and analyzed at 2 or 4h p.i. with *S*.Tm$^{SopE}$ (MOI=40; Volocity quantitation module). **A)** Association of Rab5, **B)** Rab7 and **C)** Lamp1 to T2-*gfp*$^{+}$ *S*.Tm$^{SopE}$ in *atg5*$^{+/+}$ and *atg5*$^{-/-}$ MEF. **D)** Association of Rab5, **E)** Rab7 and **F)** Lamp1 to *S*.Tm$^{SopE}$ expressing constitutive GFP in *atg5*$^{+/+}$ and *atg5*$^{-/-}$ MEF. All data were from ≥2 independent experiments. Circles=average fluorescence (AU=arbitrary unit) around 10 randomly picked *S*.Tm (mean and SEM). **G)** Representative fluorescence microscopy image of *atg5*$^{+/+}$ MEF at 2h p.i. with *S*.Tm$^{SopE}$. Orange=stable LC3-RFP; green=transiently expressed Rab7-GFP; red=α-LPS-CY5 antibody staining "all" *S*.Tm$^{SopE}$. Bar=5µm.

**Figure 4: Time course of SCV maturation in *S*.Tm$^{\Delta T2}$ infected cells.** *Atg5*$^{+/+}$ or *atg5*$^{-/-}$ MEF were infected with *S*.Tm$^{\Delta T2}$ (T2-*gfp* assay (1-12h p.i.; MOI=40). Data were from ≥6 independent experiments (dots: data point; whisker bar=mean and SD).

**Figure 5: Time course of SCV maturation in *S*.Tm$^{\Delta T1}$ infected cells. A)** *Atg5*$^{+/+}$ or *atg5*$^{-/-}$ MEF were infected with a mixture of *S*.Tm$^{SopE}$ ("helper"; trigger ruffles; no *gfp* plasmid; MOI=40-60) and *S*.Tm$^{\Delta T1}$ (T2-*gfp* reporter; MOI=150-250). T2-*gfp* expression was analyzed as above (Fig. 2E). Data were from ≥6 independent experiments. **B)** Gentamicin-protection assay time course with a mixture of *S*.Tm$^{SopE}$ ("helper"; no *gfp* plasmid; MOI=8) and *S*.Tm$^{\Delta T1}$ (T2-*gfp* reporter; MOI=40). Pathogen loads were determined by plating. **C)** Intracellular growth ([cfu (6h p.i.)]/[cfu (2h p.i.]); data from B. Dots: data points; whisker bar=mean and SD.

**Figure 6: Autophagy impact on the T1-expressing *S*.Tm subpopulation. A)** Representative images of *atg5*$^{+/+}$ or *atg5*$^{-/-}$ MEF stably expressing LC3-GFP at 40min p.i. with *S*.Tm$^{SopE}$ (constitutive mCherry; MOI≈30); bar=10µm. **B)** Time course of LC3-GFP recruitment to *S*.Tm$^{SopE}$ (constitutive mCherry; 40-240min p.i.; MOI≈30). **C)** LC3-GFP recruitment to *S*.Tm$^{SopE}$ at MOI=1 or 10 (constitutive mCherry 40min p.i.). **D)** LC3-RFP recruitment in *atg5*$^{+/+}$ MEF to *S*.Tm$^{SopE}$ at MOI=1 or 10 at 2h p.i.. Green=data for T2-*gfp* expressing *S*.Tm$^{SopE}$; Grey=data for *S*.Tm$^{SopE}$ expressing constitutive GFP. Data are from ≥2 independent experiments. Dots=average LC3 fluorescence (AU=arbitrary unit) per 10 *S*.Tm; whisker bar=mean and SEM.

**Figure 7. Fluid phase marker retention in the SCV. A)** *Atg5*$^{+/+}$ or *atg5*$^{-/-}$ MEF were incubated with 500kDa FITC-dextran during a 90 min infection with *S*.Tm$^{SopE}$ (constitutive mCherry; MOI=40) or *S*.Tm$^{\Delta T1}$ (constitutive mCherry, MOI=150; unlabeled helper strain=*S*.Tm$^{SopE}$). The FITC-dextran signal surrounding *S*.Tm$^{SopE}$ or *S*.Tm$^{\Delta T1}$ was quantified. Right side: same as left side, but using Gal3-mOrange expressing MEF and α-LPS-staining to detect

*S*.Tm$^{SopE}$. **B)** Osmotic shock assay. *Atg5*$^{+/+}$ or *atg5*$^{-/-}$ MEF expressing Gal3-mOrange were incubated with 500kDa Blue-dextran during a 90 min infection with *S*.Tm$^{\Delta T1}$ (constitutive GFP) internalized via HGF-treatment. No infection = background; osmotic shock was inflicted after 57min, i.e. by 10min 0.5M sucrose (PBS, 10%PEG1000), 3min in 60% PBS and 20min recovery in culture media. The Blue-dextran signal surrounding *S*.Tm$^{\Delta T1}$ was quantified. Extracellular *S*.Tm$^{\Delta T1}$, identified by α-LPS antibodies, were excluded from analysis. **C)** Representative images from B. bar=10µm. **D)** Model depicting the novel role of autophagy in promoting repair of T1-damaged endosome membranes Red: T1-expressing *S*.Tm; grey: *S*.Tm w/o T1 expression. Green: T2 expression. Yellow: autophagy proteins.

# Figure 1

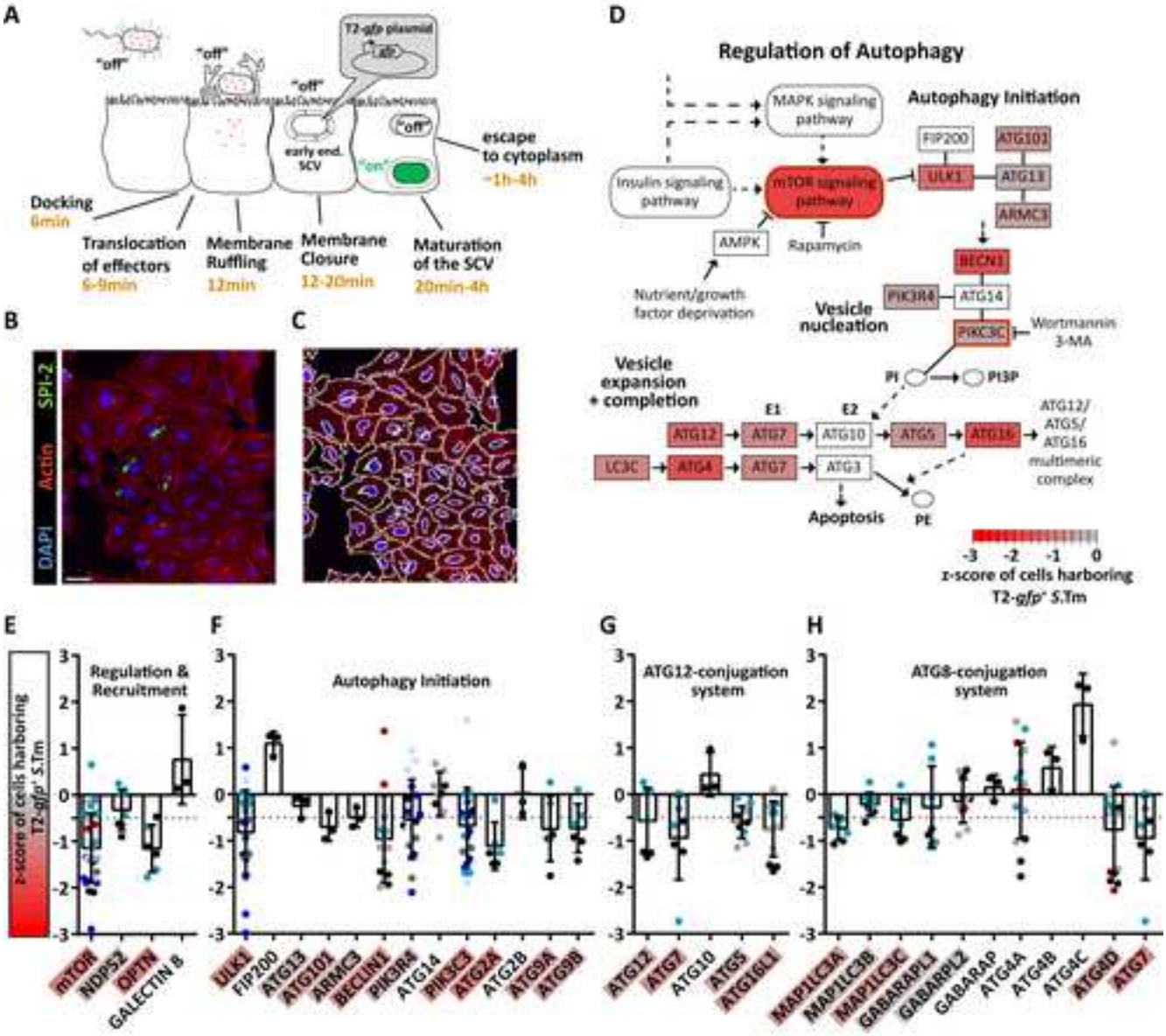

# Figure 2

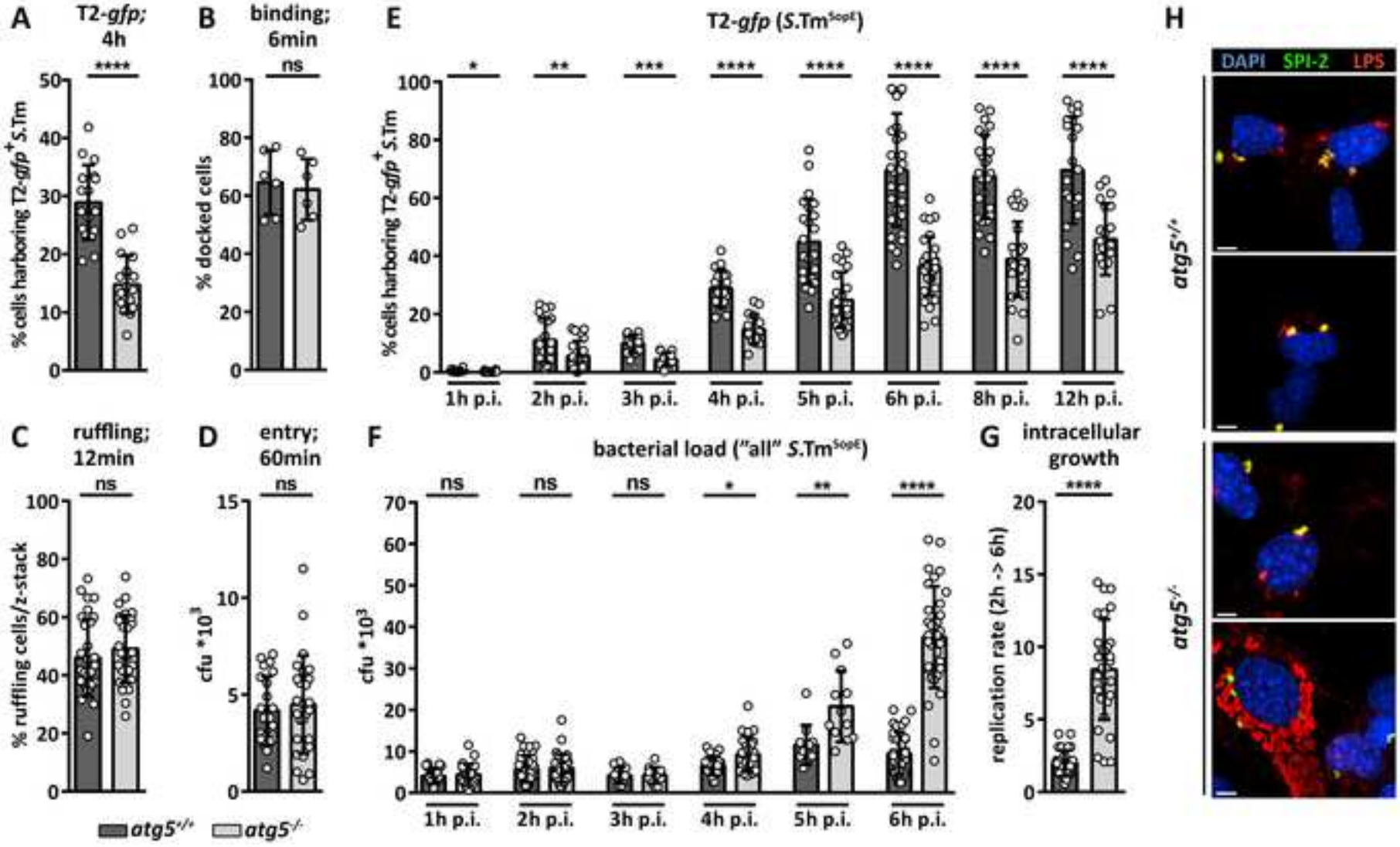

# Figure 3

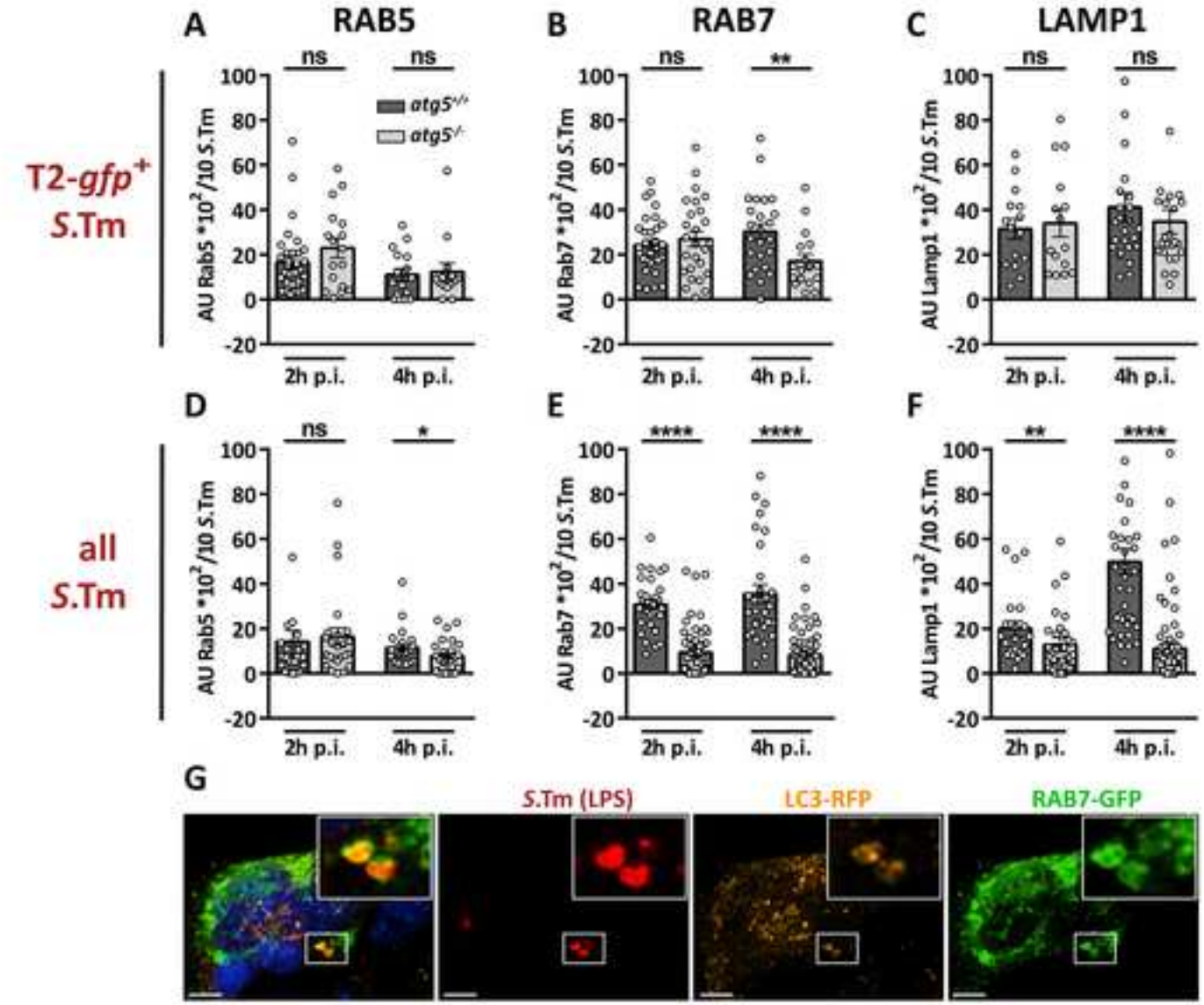

Click here to download Figure Figure 4.tif

# Figure 4

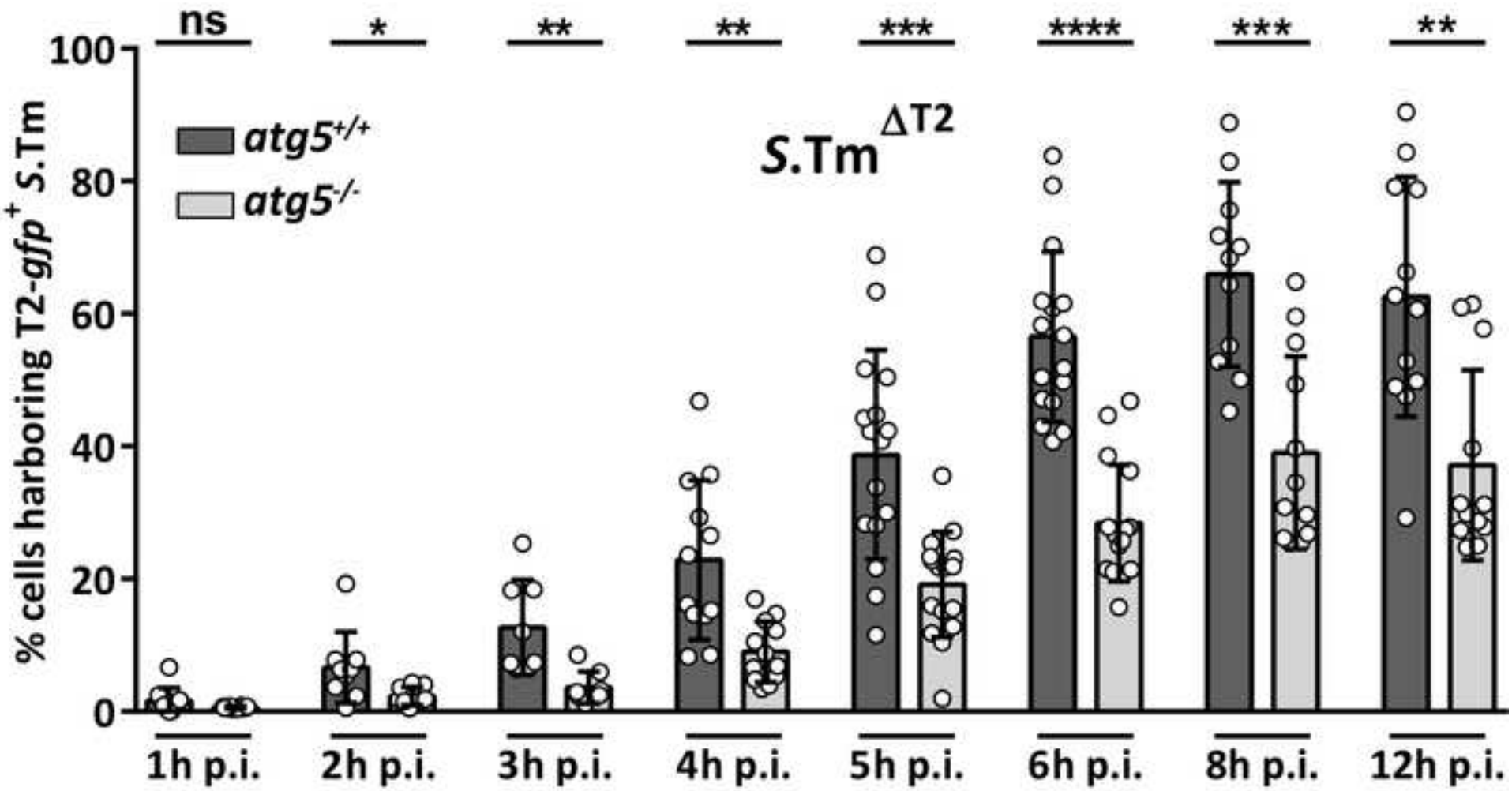

# Figure 5

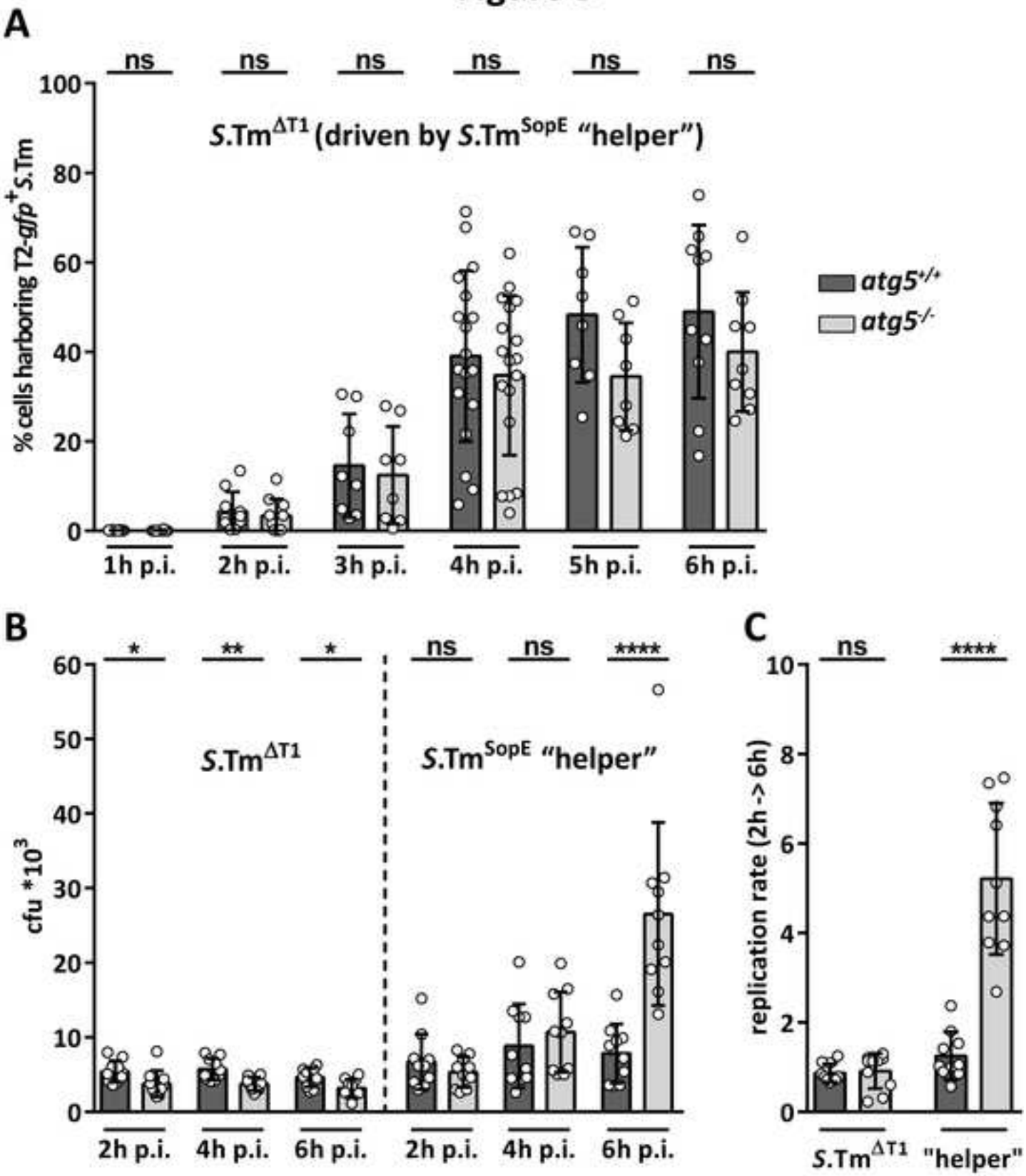

# Figure 6

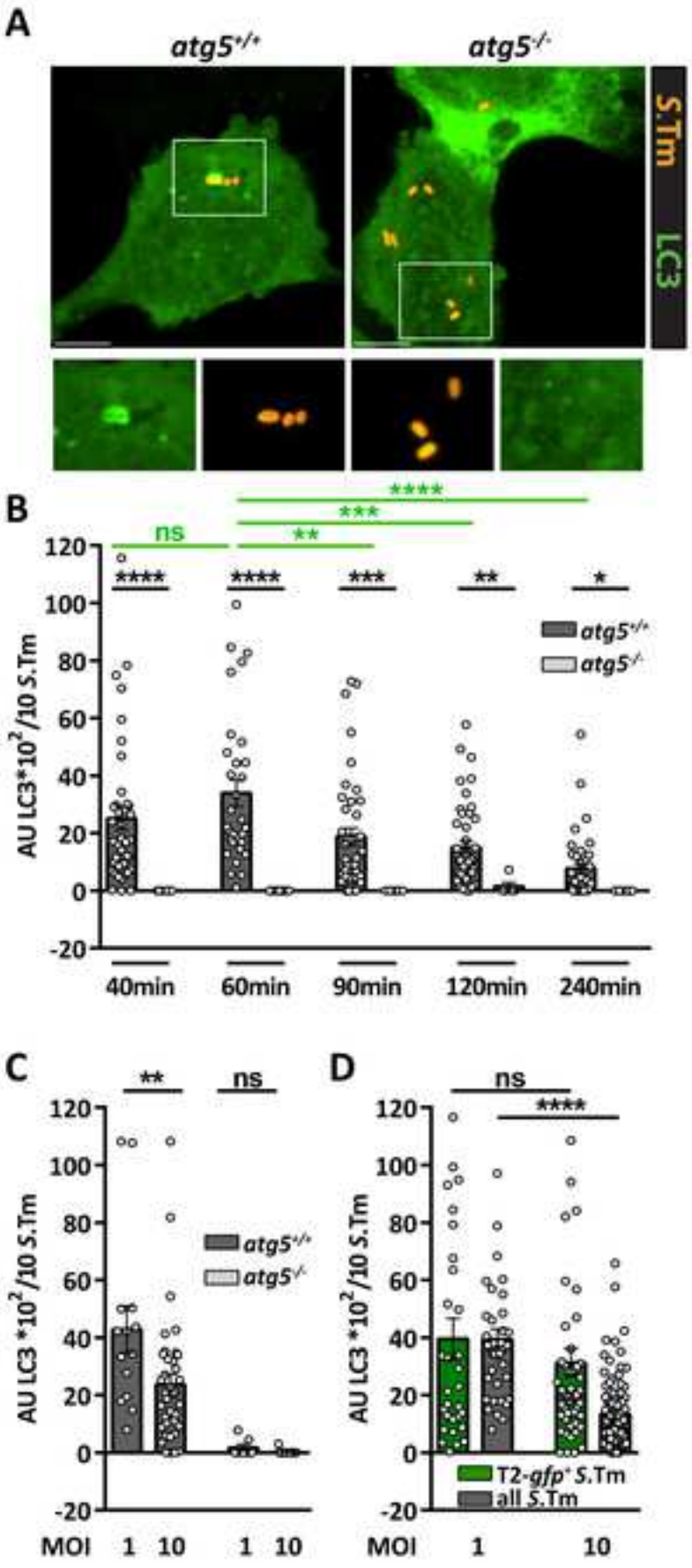

# Figure 7

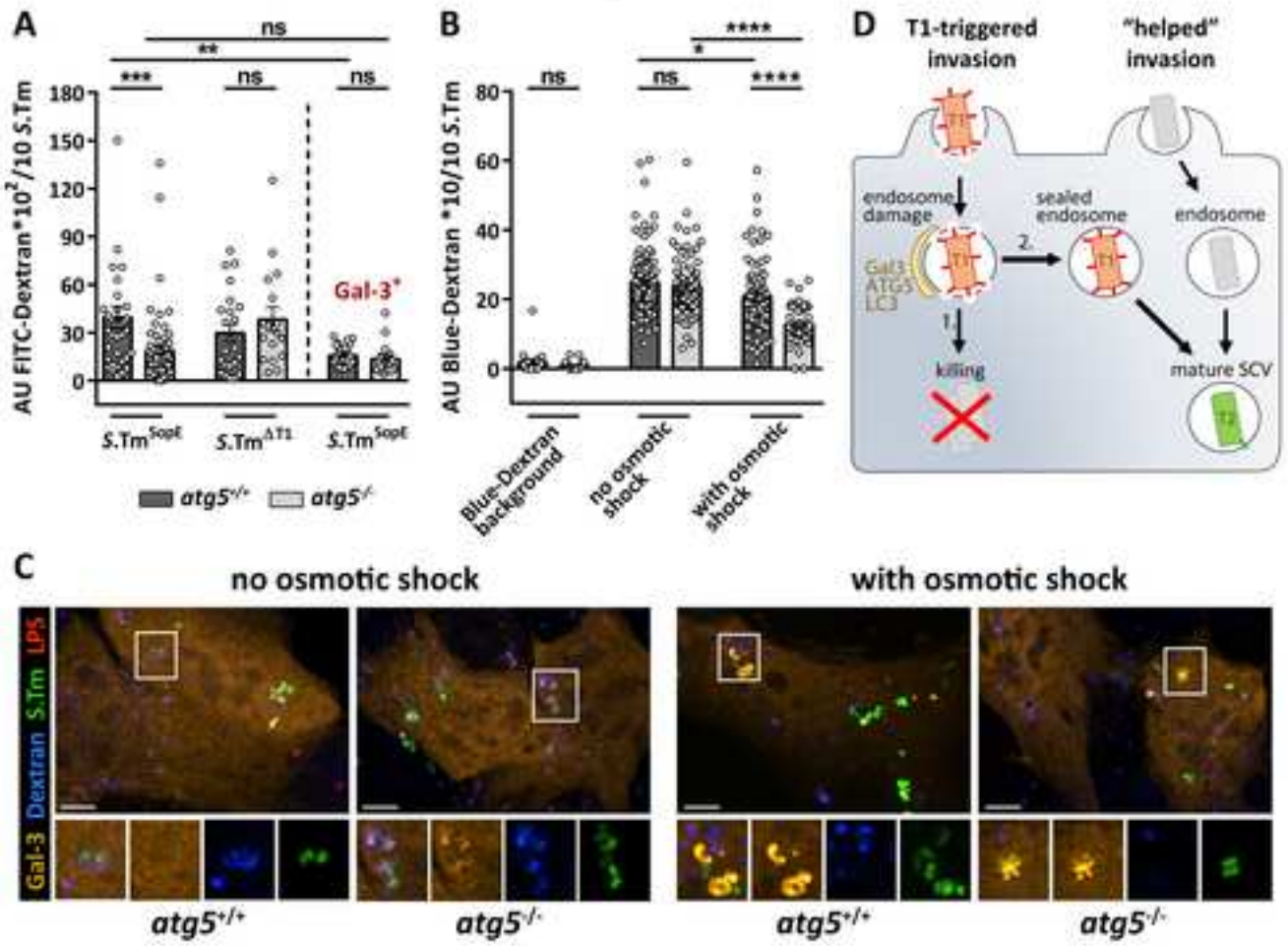

# Supplemental Data

**Figure S1, related to Figure 1: The specificity of the T2-*gfp* reporter assay for SCV-residing *S*.Tm. A)** The endosomal acidification inhibitor Bafilomycin (200nM) was used to test its impact on the T2-*gfp* reporter assay at the indicated time points of *S*.Tm infection in HeLa cells (-1 = 1h before infection; 0 = together with infection; +1, +2, +3 = hours post infection; MOI=80). The data are normalized to the *S*.Tm$^{SopE}$ infection rate of mock-treated cells and show a severe reduction of T2-induction when applied at the early stage of *S*.Tm infection. The results are derived from three independent experiments each consisting of two biological replicates. Individual data points are shown as circular symbols with their corresponding mean (bar) and SD. Stippled line: cut-off for defining the functionally important effects. **B)** Lamp1-expressing MEF were analyzed for the frequency of Lamp1 association to T2-*gfp*$^+$ and T2-*gfp*$^-$ *S*.Tm$^{SopE}$ (MOI=40) at 2 and 4h p.i. **C)** The recruitment of Ubiquitin to intracellular *S*.Tm$^{SopE}$ (MOI=40) was analyzed over the course of infection (2, 3, 4 and 6h p.i.) in *atg5*$^{+/+}$ and *atg5*$^{-/-}$ cells. The associated Ubiquitin signal (top panels) was separately quantified for "all" *S*.Tm (constitutive GFP; left side) and T2-*gfp*$^+$*S*.Tm (right side), which allowed to obtain the relative frequency of Ubiquitin association to these different *S*.Tm subpopulations (bottom panels). Data are derived from four independent experiments. The average Ub fluorescence (AU = arbitrary unit) per 10 *S*.Tm is shown as circles. Bar: overall mean. The SEM is indicated. The frequency of Ub association is determined per 100 *S*.Tm (circles) and shown with their mean and SD. **D)** *S*.Tm$^{SopE}$-infected HeLa cells (MOI=50) were fixed at 4h p.i. and prepared for correlative light/electron microscopy according to the standard Tokuyasu techniques (Oorschot et al., 2014). Left panel: Light microscopy (LM) with immunofluorescence of Lamp1 (Red) and a GFP antibody against the T2-*gfp* reporter. Middle panel: Electron microscopy (EM). Right panel: Alignment of EM and LM using the Amira software. Scale bar of whole cell = 2µm; scale bar enlarged top images = 500nm. **E)** Effect of control siRNAs on the viability (number) of cells. Strong cytotoxicity was observed for all Kif11-treated wells, whereas the pathogen-specific controls and wells transfected with mock- or scrambled RNA had no or only slight effects on the cell numbers. **F)** Z-scored infection by T2-*gfp*$^+$ *S*.Tm of cells treated with siRNA controls in comparison to mock- and scrambled-treated wells. Reduction of cell numbers in Kif11-treated wells led to a strong increase of cells harboring T2-*gfp*$^+$ *S*.Tm. This was already observed in earlier work and is attributable to the enhanced infection efficiency of rounded cells (Misselwitz et al., 2012). The pathogen-specific controls ARPC3, CDC42 and ATP6V1A led to a pronounced impairment of T2-*gfp*$^+$ *S*.Tm infection, whereas knockdown of CFL1 and ITGAV resulted in slightly enhanced phenotypes. This is well in line with previous work (Misselwitz et al., 2011a). All data points refer to individual, siRNA-treated wells from three replicates of the genome-wide RNAi screen and their corresponding mean and SD. **G)** Results of the GWS were extracted for the KEGG pathway of Regulation of Actin Cytoskeleton (comparable to Figure 1D). Red frames: effects of the indicated inhibitors or observed in earlier screens (Qiagen; (Misselwitz et al., 2011a)). The values for Profilin (PFN) are derived from the four individual Profilin screening data (PFN1= -0.6; PFN2= -0.04; PFN3= -0.8; PFN4= -0.4).

**Figure S2, related to Figure 2: A) - D) Working model for the role of autophagy in controlling the fate of wild type and T1 mutant *S*.Tm. A)** Wt *S*.Tm infection of wt host cells. T1 triggers ruffling plus invasion and inflicts membrane damage to the early endosome. This damage is recognized by the autophagy system. This has two different consequences: 1. the tagging of *S*.Tm for degradation, a phenotype well established to limit pathogen replication in the host cell's cytosol. 2. An increased number of bacteria expressing T2. This is a new phenotype. The subsequent experiments suggest that the second, newly identified phenotype is attributable to autophagy-dependent sealing of the endosomal membrane damage, which targets these endosomes for further maturation into SCV and thereby increases the number of T2-expressing bacteria per infected cell. A fraction of the wt *S*.Tm inoculum is not expressing T1 and therefore enters the host cell by "helped" invasion. The resulting endosomes are not damaged and do not require autophagy for maturation into SCV. **B)** Wt *S*.Tm infection of autophagy-deficient host cells. Here, both autophagy-mediated effects are alleviated. Therefore, the T1-expressing bacteria do access the host cellular cytosol in large numbers and hyper-replicate. In addition, the endosome is not sealed. This reduces the number of mature SCVs harboring T2-expressing bacteria. *S*.Tm cells entering by "helped" invasion are handled as in wt host cells. **C)** and **D)** Infection by T1 mutant bacteria. This can only occur via "helped

invasion" or by Invasin expression (see, below). The endosome membrane remains intact. Therefore, there is little/no escape into the cytosol and the number of properly matured SCVs and the number of cells harboring T2-expressing bacteria is equivalent in wild type and in autophagy-deficient host cells. Red: T1-expressing *S*.Tm cell; gray: *S*.Tm cell expressing neither T1 nor T2. Green: *S*.Tm cell expressing T2. This does only occur upon SCV maturation and proper acidification. Yellow: proteins of the autophagy system. **E - F) Expulsion assay of *S*.Tm$^{SopE}$-infected *atg5*$^{+/+}$ and *atg5*$^{-/-}$ cells. E)** Initial cfu recovered at 1h p.i. (MOI=80) are shown to define the rate of expelled bacteria after the addition of trimethoprim (25µg/ml) and α-methyl-mannose (100mM) as reported before (Miao et al., 2015). **F)** Expelled cfu were determined at 4.4 - and 6.4h p.i. in *atg5*$^{+/+}$ and *atg5*$^{-/-}$ cells. Due to low numbers of recovered bacteria, the expulsion rate is not shown (<1%). **G) - H) The role of *atg5* during wt *S*.Tm infections. G)** *atg5*$^{+/+}$ and *atg5*$^{-/-}$ cells were infected for the indicated times with wt *S*.Tm carrying the T2-*gfp* reporter (MOI=40). The reporter expression was analyzed by automated microscopy as described in Figure 1 and Figure 2. **H)** Gentamicin-protection assay (MOI=10) was performed to analyze pathogen loads in the host cell cytoplasm at 2h and 6h p.i. in *atg5*$^{+/+}$ and *atg5*$^{-/-}$ cells. The intracellular replication rate was calculated from these values. Circles illustrate the individual data points and the bars present their mean with corresponding SD. **I) Phenotype of autophagy-related knockdowns on *S*.Tm binding.** HeLa cells were transfected with a targeted library of autophagy-related hits (Qiagen; 3 to 5 individual siRNAs per gene). To assess the impact of respective knockdowns on binding, cells were infected with the non-invasive *S*.Tm$^{\Delta 4}$ mutant (MOI=125) for 6min and subsequently stained for analysis by indirect immunofluorescence microscopy. Data are grouped according to the function of the analyzed gene. Data are derived from five independent experiments and are shown as log2 docking values normalized to mock-treated wells. Circles illustrate the individual data points per siRNA and bars present the mean with corresponding SD. **J) - K)** Single cell analysis for the numbers of T2-*gfp*$^{+}$ **(J)** and T2-*gfp*$^{-}$ **(K)** *S*.Tm$^{SopE}$ (MOI=40) harbored per infected *atg5*$^{+/+}$ or *atg5*$^{-/-}$ cell; determined through manual quantification.

**Figure S3, related to Figure 3: A)** Bafilomycin treatment in *atg5*$^{+/+}$ and *atg5*$^{-/-}$ cells, which was added at distinct time points during *S*.Tm$^{SopE}$ infection (MOI=40; see Figure S1A). The data were normalized to the mock-treated infection rate of *S*.Tm$^{SopE}$ in *atg5*$^{+/+}$ cells and are derived from at least three independent experiments each consisting of two biological replicates. Individual data points are shown as circular symbols with their corresponding mean (bar) and SD. **B)** Co-localization of constitutively active or dominant negative Rab7 with *S*.Tm during infection of *atg5*$^{+/+}$ and *atg5*$^{-/-}$ cells. To measure the association of distinct Rab7 versions with *S*.Tm$^{SopE}$, host cells were transfected with expression plasmids for constitutively active (CA; RAB7Q67L) or inactive (DN; RAB7T22N) Rab7. The cells were subsequently infected for 2h or 4h with *S*.Tm$^{SopE}$ (MOI=60). Fluorescence microscopy was used to quantify the co-localization of the Rab7 constructs with "all" *S*.Tm$^{SopE}$ (constitutive mCherry) in *atg5*$^{+/+}$ and *atg5*$^{-/-}$ cells. Data are derived from at least three independent experiments and the circles represent the mean Rab7 fluorescence (AU = arbitrary unit) per 10 *S*.Tm with the overall mean of the experiment (bar) and their respective SEM. **C) - D) The role of Rab5 in infection- and LC3 association with *S*.Tm. C)** HeLa cells were treated with siRNAs (4 distinct siRNAs per gene, Qiagen) directed against Rab5A, B and/or C as indicated. The cells were infected for 4h with *S*.Tm$^{SopE}$ (MOI=60) and the efficiency of SCV maturation was assessed by automated microscopy quantifying the expression of the T2-*gfp* reporter. The data are displayed as log2 values of cells harboring T2-*gfp*$^{+}$ *S*.Tm in relation to mock-treated wells. Circles illustrate the individual data points per siRNA and bars present the mean with corresponding SD for the independent experiments performed (n=2-5). **D)** LC3 recruitment was assessed at 1h p.i. as described in Figure 6. Data are derived from two independent experiments and circles represent the mean fluorescence LC3 signal (AU = arbitrary unit) measured around 10 *S*.Tm, with their mean (bars) and SEM.

**Figure S4, related to Figure 5: A) - C) Analysis of Lamp1 association during the helper assay. A)** Representative images of Lamp1-(cherry) expressing cells infected with *S*.Tm$^{\Delta T1}$ (LPS staining; MOI=150) through the helper strain *S*.Tm$^{SopE}$ (constitutive GFP; MOI=16) at 2h p.i. Enlarged image sections show that both *S*.Tm strains (helper and T1 mutant) can be found in separated Lamp1-positive vacuoles, as indicated by white arrows. **B)** Quantified frequency of Lamp1 around separated *S*.Tm$^{SopE}$ (constitutive GFP) in a helper assay with *S*.Tm$^{\Delta T1}$ at 2h p.i.. **C)** Quantified frequency of Lamp1 around separated *S*.Tm$^{\Delta T1}$ (constitutive GFP) in a helper assay with *S*.Tm$^{SopE}$ at 2h p.i.. **D) - F) The impact of *atg5* during Invasin-mediated infection of *S*.Tm$^{\Delta T1}$.** The *Yersinia pseudotuberculosis*-

derived adhesin Invasin was used to facilitate invasion of the *S*.Tm$^{\Delta T1}$ mutant by a zipper-like mechanism. **D)** The mutant (*S*.Tm$^{\Delta T1 + Invasin}$; MOI~120) was used to infect *atg5*$^{+/+}$ and *atg5*$^{-/-}$ cells for the indicated times as described in Figure 5. The infection was analyzed using the automated microscopy assay. **E)** Gentamicin-protection assay. Cells were infected for 2, 4 or 6h with *S*.Tm$^{\Delta T1 + Invasin}$ (MOI~40) and the intracellular pathogen loads were analyzed by plating. In both cell types (*atg5*$^{+/+}$ and *atg5*$^{-/-}$), the intracellular pathogen loads remained constant throughout the time of the experiment. **F)** Intracellular replication rate derived from the data shown in panel E. Data are derived from at least five independent experiments. Circles illustrate the individual data points and the bars present their mean with corresponding SD.

**Figure S5, related to Figure 6: A) - B) Recruitment of LC3 during the course of a "helped" *S*.Tm$^{\Delta T1}$ infection**. To measure and quantify the association of the marker protein LC3 with intracellular *S*.Tm$^{\Delta T1}$, *atg5*$^{+/+}$ and *atg5*$^{-/-}$ cells (stable lentiviral LC3 expression) were infected with *S*.Tm$^{\Delta T1}$ (MOI=200; constitutive mCherry) through a "helped" infection with *S*.Tm$^{SopE}$ (MOI=40; unlabeled) for 30min. At subsequent time points (40min, 60min, 90min, 120min and 240min) the association of LC3 to *S*.Tm$^{\Delta T1}$ was quantified by fluorescence microscopy. **A)** A representative image for LC3 association showing that there was no efficient recruitment of LC3 to *S*.Tm$^{\Delta T1}$ neither in *atg5*$^{+/+}$ nor in *atg5*$^{-/-}$ cells at 1hpi. Scale bar = 10µm. **B)** Quantitative analysis of LC3 recruitment to *S*.Tm$^{\Delta T1}$ during the course of infection. Data are derived from three independent experiments. Circles represent the average fluorescence signal (AU = arbitrary unit) of LC3 per 10 *S*.Tm with their corresponding overall mean (bar) and SEM. **C) - E) Galectin-3 associates with wt *S*.Tm, but not with *S*.Tm$^{\Delta T1}$.** To verify that T1 compromises the SCV integrity, we employed the vacuolar damage marker Galectin-3. Galectin-3 belongs to a family of cytosolic "danger receptors", which can detect endosome rupture (Paz et al., 2010; Thurston et al., 2012). *atg5*$^{+/+}$ cells were transfected with a Galectin-3-GFP expression plasmid and infected with either *S*.Tm$^{SopE}$ (constitutive mCherry) or a "helped" infection of *S*.Tm$^{\Delta T1}$ (constitutive mCherry + the unlabeled helper strain *S*.Tm$^{SopE}$). **C)** Representative fluorescence microscopy images of Galectin-3-expressing *atg5*$^{+/+}$ cells infected with *S*.Tm$^{SopE}$ (left) or *S*.Tm$^{\Delta T1}$ (right) at 40min post infection. Recruitment of Galectin-3 to an *S*.Tm subpopulation was only detected in the case of *S*.Tm$^{SopE}$ infection (see enlarged white boxes). Scale bar = 5µm. **D)** Time course (40min, 60min, 90min, 120min and 240min) of Galectin-3 recruitment during *S*.Tm$^{SopE}$ or *S*.Tm$^{\Delta T1}$ infection in *atg5*$^{+/+}$ cells. **E)** MOI-dependence of Galectin-3 recruitment to *S*.Tm$^{SopE}$ in *atg5*$^{+/+}$ cells at 40min post infection. The data are derived from five independent experiments; circles show the average Galectin-3 fluorescence signal (AU = arbitrary unit) per 10 *S*.Tm as well as their overall mean (bar) with SEM.

**Figure S6, related to Figure 7: Osmotic damage results in Ubiquitin association around T2-*gfp*$^{+}$ *S*.Tm.** MEFs were infected with either **A)** *S*.Tm$^{SopE}$ (20min; MOI=40) or **B)** *S*.Tm$^{\Delta T1}$ (HGF-induced internalization for 60min; MOI=120). 90min after infection, the cells were exposed to osmotic damage (see (Thurston et al., 2012)). Fixation took place at 2 h p.i. and the signal of Ubiquitin association to T2-*gfp*$^{+}$ *S*.Tm$^{SopE}$ **(A)** or *S*.Tm$^{\Delta T1}$ **(B)** was compared to the unperturbed cells infected for 2h (see Figure S1C).

## Figure S1

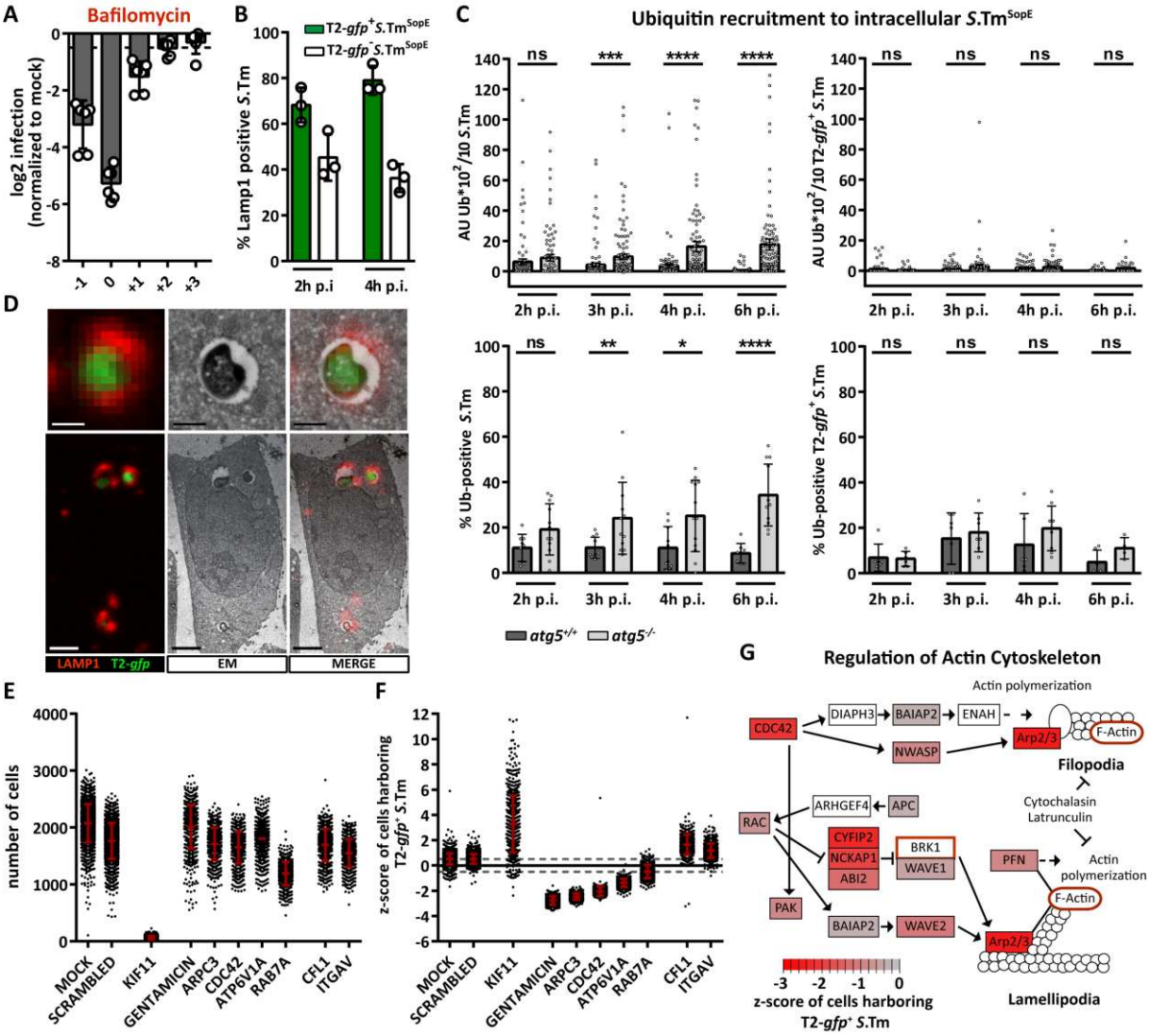
A
Bafilomycin
log2 infection (normalized to mock)
B
T2-gfp+ S.TmSopE
T2-gfp- S.TmSopE
% Lamp1 positive S.Tm
2h p.i
4h p.i.
C
Ubiquitin recruitment to intracellular S.TmSopE
AU Ub*10²/10 S.Tm
AU Ub*10²/10 T2-gfp+ S.Tm
% Ub-positive S.Tm
% Ub-positive T2-gfp+ S.Tm
2h p.i.
3h p.i.
4h p.i.
6h p.i.
ns
atg5+/+
atg5-/-
D
LAMP1 T2-gfp
EM
MERGE
E
number of cells
MOCK
SCRAMBLED
KIF11
GENTAMICIN
ARPC3
CDC42
ATP6V1A
RAB7A
CFL1
ITGAV
F
z-score of cells harboring T2-gfp+ S.Tm
G
Regulation of Actin Cytoskeleton
Actin polymerization
CDC42
DIAPH3
BAIAP2
ENAH
Arp2/3
F-Actin
NWASP
Filopodia
Cytochalasin
Latrunculin
ARHGEF4
APC
RAC
CYFIP2
NCKAP1
ABI2
BRK1
WAVE1
PFN
Actin polymerization
F-Actin
PAK
BAIAP2
WAVE2
Arp2/3
Lamellipodia
z-score of cells harboring T2-gfp+ S.Tm

## Figure S2

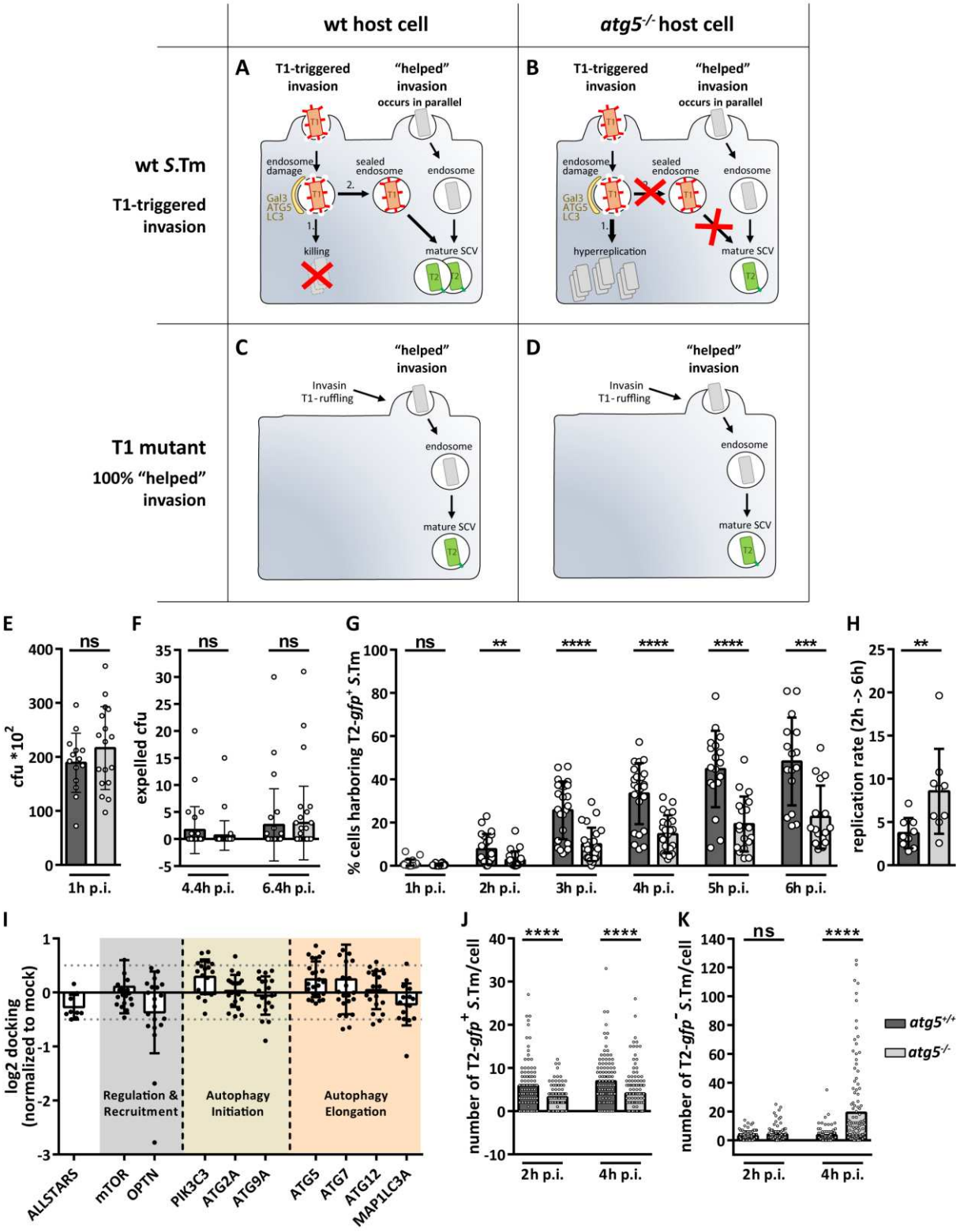
wt host cell
atg5-/- host cell
A
B
C
D
wt S.Tm
T1-triggered invasion
T1 mutant
100% "helped" invasion
T1-triggered invasion
"helped" invasion
occurs in parallel
endosome damage
sealed endosome
endosome
Gal3 ATG5 LC3
killing
mature SCV
hyperreplication
Invasin T1-ruffling
E
F
G
H
cfu *10^2
expelled cfu
% cells harboring T2-gfp+ S.Tm
replication rate (2h -> 6h)
ns
**
***
****
1h p.i.
4.4h p.i.
6.4h p.i.
2h p.i.
3h p.i.
4h p.i.
5h p.i.
6h p.i.
I
J
K
log2 docking (normalized to mock)
Regulation & Recruitment
Autophagy Initiation
Autophagy Elongation
ALLSTARS
mTOR
OPTN
PIK3C3
ATG2A
ATG9A
ATG5
ATG7
ATG12
MAP1LC3A
number of T2-gfp+ S.Tm/cell
number of T2-gfp- S.Tm/cell
atg5+/+
atg5-/-

**Figure S3**

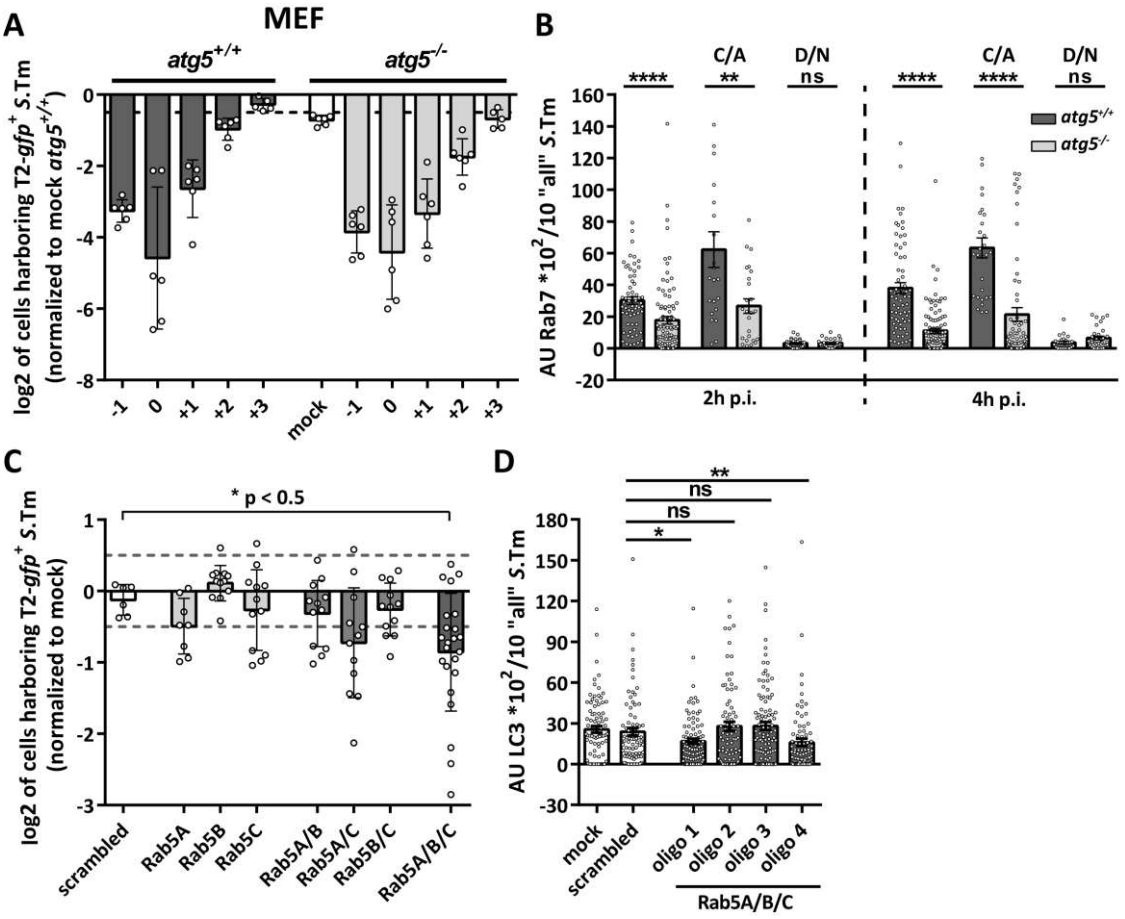
A
MEF
atg5+/+
atg5-/-
log2 of cells harboring T2-gfp+ S.Tm (normalized to mock atg5+/+)
-1
0
+1
+2
+3
mock
B
C/A
D/N
****
**
ns
atg5+/+
atg5-/-
AU Rab7 *10^2/10 "all" S.Tm
2h p.i.
4h p.i.
C
* p < 0.5
log2 of cells harboring T2-gfp+ S.Tm (normalized to mock)
scrambled
Rab5A
Rab5B
Rab5C
Rab5A/B
Rab5A/C
Rab5B/C
Rab5A/B/C
D
**
ns
*
AU LC3 *10^2/10 "all" S.Tm
mock
scrambled
oligo 1
oligo 2
oligo 3
oligo 4
Rab5A/B/C

## Figure S4

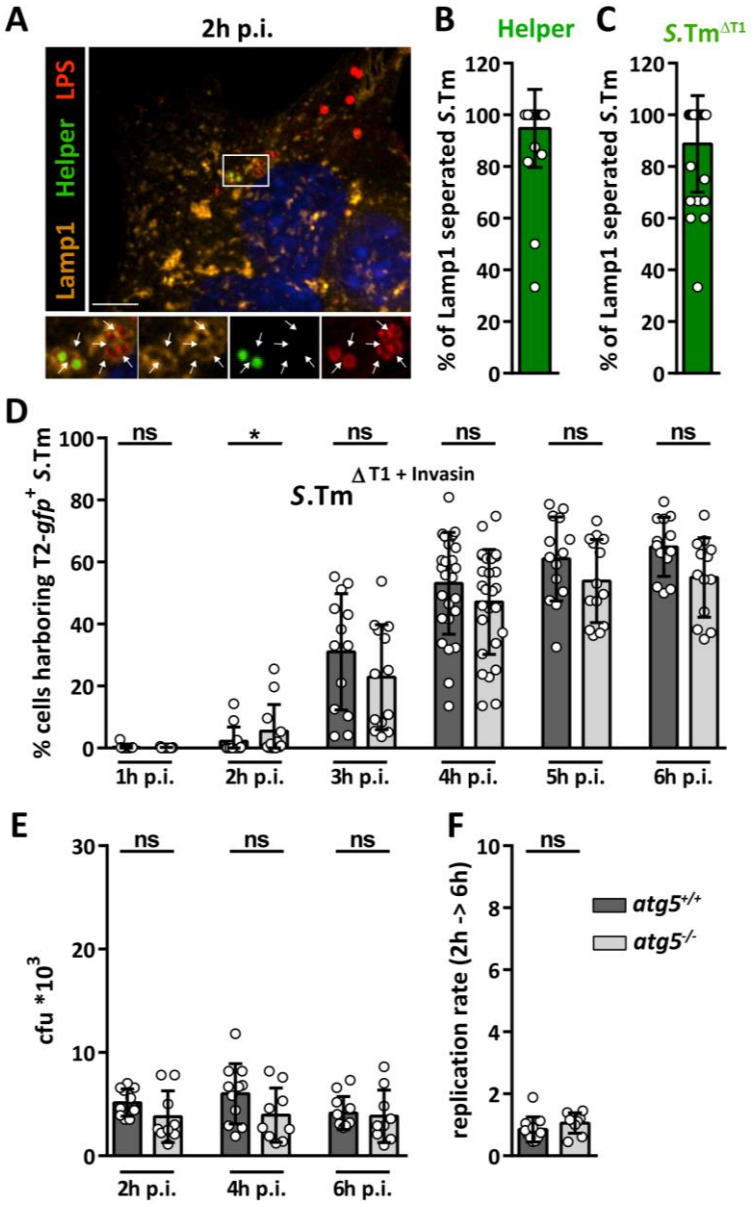
A
2h p.i.
Lamp1
Helper
LPS
B
Helper
% of Lamp1 seperated S.Tm
C
S.Tm^ΔT1
% of Lamp1 seperated S.Tm
D
% cells harboring T2-gfp+ S.Tm
S.Tm
ΔT1 + Invasin
ns
*
1h p.i.
2h p.i.
3h p.i.
4h p.i.
5h p.i.
6h p.i.
E
cfu *10^3
2h p.i.
4h p.i.
6h p.i.
F
replication rate (2h -> 6h)
atg5+/+
atg5-/-

## Figure S5

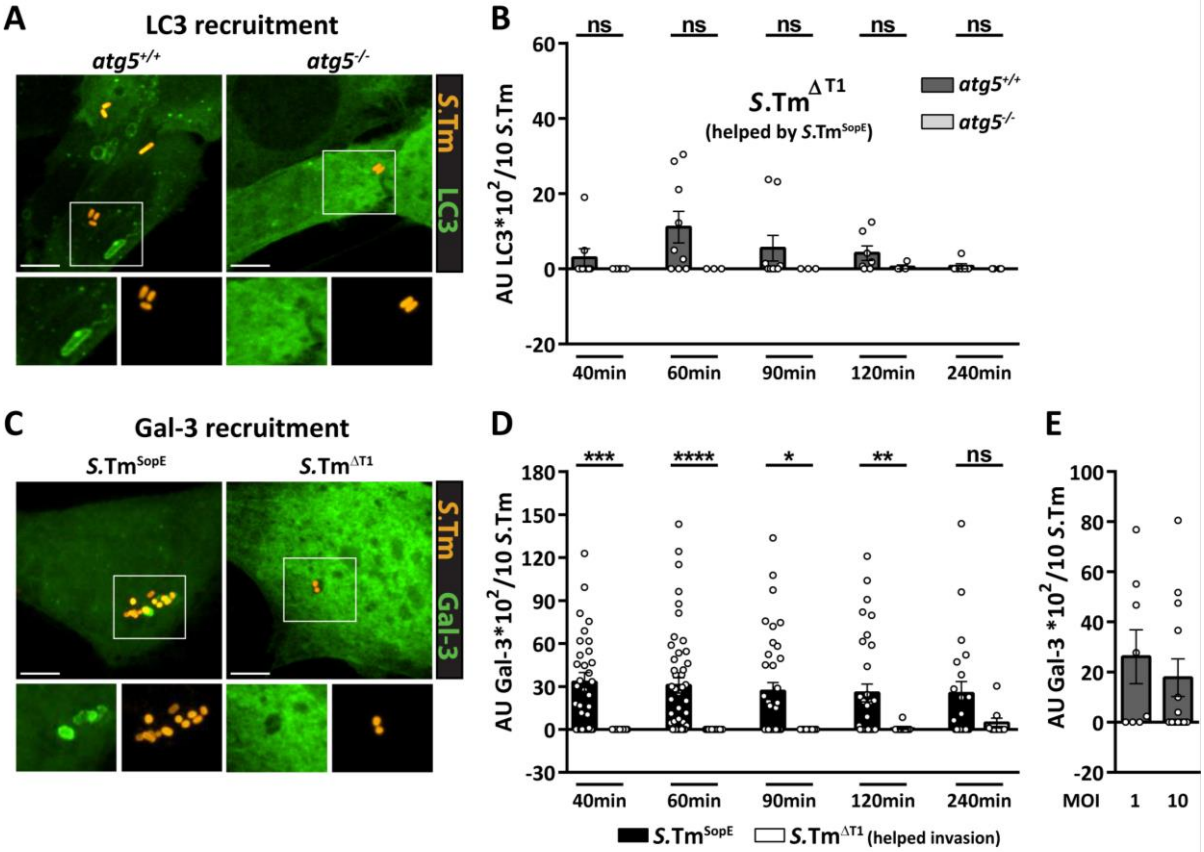
A
LC3 recruitment
atg5+/+
atg5-/-
S.Tm
LC3
B
ns
S.Tm ΔT1
(helped by S.TmSopE)
atg5+/+
atg5-/-
AU LC3*10²/10 S.Tm
40min
60min
90min
120min
240min
C
Gal-3 recruitment
S.TmSopE
S.TmΔT1
S.Tm
Gal-3
D
***
****
*
**
ns
AU Gal-3*10²/10 S.Tm
S.TmSopE
S.TmΔT1 (helped invasion)
E
AU Gal-3 *10²/10 S.Tm
MOI
1
10

## Figure S6

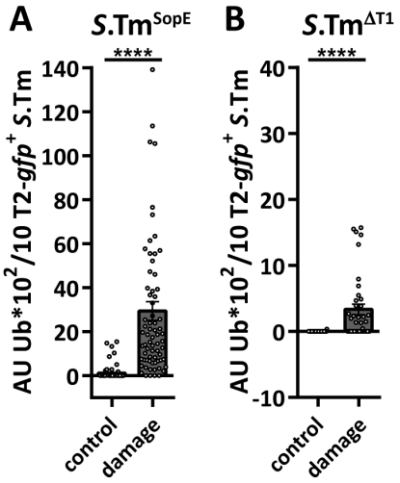
A
S.Tm^SopE
****
AU Ub*10^2/10 T2-gfp^+ S.Tm
140
120
100
80
60
40
20
0
control
damage
B
S.Tm^ΔT1
****
40
30
20
10
0
-10
control
damage

**Table S1A: Details of the S.Tm strains used in this study**

| Designation | Strain | Genotype | Reference |
|---|---|---|---|
| *S*.Tm | SB300[a] | SL1344 (wt) | (Hoiseth and Stocker, 1981) |
| *S*.Tm$^{SopE}$ | M701[b] | Δ*sopE2, ΔsopB, ΔsipA* | (Muller et al., 2009) |
| *S*.Tm$^{SopE}$ | M2421[b] | Δ*sopE2, ΔsopB, ΔsipA* | (Hoffmann et al., 2010) |
| *S*.Tm$^{SipA}$ | M516[c] | Δ*sopE, ΔsopE2, ΔsopB* | (Mirold et al., 2001) |
| *S*.Tm$^{\Delta 4}$ | M566 | Δ*sopE, ΔsopE2, ΔsopB, ΔsipA* | (Ehrbar et al., 2003) |
| *S*.Tm$^{\Delta T1}$ | SB161 | Δ*invG* | (Kaniga et al., 1994) |
| *S*.Tm$^{\Delta T2}$ | M556 | Δ*sseD* | (Hapfelmeier et al., 2004) |

[a] wild type *S*.Tm employs four different T1 effectors (SopE, SipA, SopE2, SopB) to efficiently trigger membrane ruffles and invade into HeLa cells.

[b] *S*.Tm$^{SopE}$ relies largely on the T1 effector protein SopE, a G-nucleotide exchange factor for Rac1 and Cdc42, to trigger ruffling and host cell invasion (Hardt et al., 1998; Misselwitz et al., 2011a).

[c] *S*.Tm$^{SipA}$ invasion relies largely on the T1 effector protein SipA which binds and polymerizes actin directly.

# Supplemental Experimental Procedures

**Bacterial strains and plasmids**

All *S*.Tm strains were isogenic derivatives of SL1344 (SB300), belonging to *Salmonella enterica* ssp. *enterica* serovar Typhimurium (*S*.Tm) (Hoiseth and Stocker, 1981); Genome re-sequenced (Diard et al., 2013) (Table S1A). Plasmids used for expression in *S*.Tm were pM965 (Stecher et al., 2004); pM975 (Hapfelmeier et al., 2005) and pWRG435 (Bender et al., 2013). Plasmids used for transfection into eukaryotic cells were Rab5A, Rab7, Rab7Q67L (CA) and Rab7T22N (DN) (Marino Zerial), Rab5Q79L (Pelkmans et al., 2004), Lamp1 (Jean Gruenberg) and Galectin-3 (Ehsani et al., 2012). When *S*.Tm were used for infection into tissue-cultured cell lines, they were grown in LB broth supplemented with 0.3M NaCl, 50 µg/ml Streptomycin (Applichem) and ½ of the standard concentration of the respective antibiotic for ensuring plasmid maintenance in all bacterial cells. A 12h (37°C) *S*.Tm culture was sub-cultured for 4h and then used for infection.

**Cell cultures**

HeLa CCL-2 cells (ATCC) and ATG5 wildtype (*atg5*$^{+/+}$) as well as knockout (*atg5*$^{-/-}$) mouse embryonic fibroblasts (Kuma et al., 2004) were grown in DMEM (PAA laboratories) supplemented with 10% inactivated FCS (Invitrogen) and 50 µg/ml Streptomycin (AppliChem) at 37°C and 5% $CO_2$.

**siRNA transfection**

Every siRNA screen consisted of screening plates and control plates (see (Ramo et al., 2014)). Screening plates contained the siRNAs targeting the host cell factors of interest. Control plates contained control siRNAs like Kif11 and were used to assess the siRNA transfection efficiency. In addition, every plate (screening and control plates) contained siRNA controls in the two outer columns. Besides transfection efficiency controls (Kif11 and scrambled), these included pathogen-specific controls like ArpC3 and Cdc42, which are known to reduce the infectivity upon silencing (Misselwitz et al., 2011a). To silence a host cell factor via RNAi, we used a reverse transfection protocol. The experiments were performed in 384- or 96-well plate formats. The 384-well plate format (Greiner-bio-one; µ-clear plate TC 384) represented the standard InfectX screening approach and contained 1.6pmol siRNA (1pmol esiRNA) diluted in 5µl RNase-free $ddH_20$ per well. 25µl RNAiMAX (Invitrogen)/DMEM (0.1µl/ 24.9µl) were added to each well and then incubated for 1h at 37°C. Afterwards, 550 HeLa CCL-2 cells in 50µl DMEM/16% FCS were seeded into each well. The siRNA plates were incubated for 72 hours at 37°C and 5% $CO_2$. When using full-size 96-well plates (µ-clear bottom, Greiner Bio One), the amounts of the different reagents were adapted to a final volume of 100µl and 2800 cells in 70µl DMEM/16% FCS. Control siRNA dilution series and cell dilution controls verified that changes in cell number of up to 6-fold did not affect the *Salmonella* infection efficiency. This was important to guarantee the robustness of our screen, as many siRNAs are known to slightly affect the cell number.

**siRNA libraries**

The genome-wide screen was performed in three independent replicates using the Dharmacon ONTARGETplus SMART pool siRNA Library targeting 18.237 genes in 57 distinct 384-well plates. Furthermore, customized siRNA libraries from Ambion/LifeTechnologies (3 Ambion Silencer Select siRNAs and 3 Ambion Silencer siRNAs for each candidate), esiRNAs (Sigma) and siRNA libraries targeting kinases and phosphatases were tested screened (3 siRNAs from Ambion/LifeTechnologies (SilencerSelect), 4 siRNAs from Dharmacon (Human ON-TARGETplus) and a pool of 4 Dharmacon siRNA's in one well (Human ON-TARGETplus SMARTpool)). All siRNAs and the screening data are shown in Table S1B. The pathogen-specific siRNAs present in every screening plate were ArpC3, Cdc42, ATP6V1A (negative effect on *S*.Tm infection) and ITGAV and CFL1 as hits that are known to enhance *S*.Tm infection (Misselwitz et al., 2011a).

**T2-*gfp* reporter assay (siRNA GWS and follow-up assays)**

For infection of siRNA screening plates, the strain *S*.Tm$^{SopE}$ (M2421, see Table S1A) was used, which harbored the plasmid pM975, a reporter for SPI-2-induced expression of GFP (*ssaG*-promotor) (Hapfelmeier et al., 2005). To perform the infection, 16µl of *S*.Tm$^{SopE}$ (MOI=80; 4h subculture diluted in DMEM) were added to the HeLa cells and incubated for 20min at 37°C and 5% $CO_2$. Afterwards, the medium was replaced by 60µl DMEM/10% FCS

containing 400µg/ml gentamicin to kill all remaining extracellular bacteria. The cells were further incubated for 3h 40min at 37°C and 5% $CO_2$ and then fixed by adding 35µl 4% PFA, 4% sucrose in PBS for 20min at RT. Then, 60µl PBS containing 400µg/ml gentamicin was used to replace the fixation solution. Permeabilization of cells was performed for 5min with 0.1% TritonX-100, which was replaced by a staining solution containing 1µg/ml DAPI (Sigma-Aldrich) and 1.2 U/ml DY-547-phalloidin (Dyomics). After an incubation of 1h at RT, the plates were washed 3x with PBS and stored for imaging using 60µl PBS containing 400µg/ml gentamicin per well (sealed with Platesealer; Greiner bio one). All liquid handing steps of infection, fixation, and immunofluorescence staining were performed on a liquid handling robot (BioTek; EL406).

Performance of this assay: The key issue of interest is the ability of the T2-*gfp* reporter to monitor SCV maturation. This has been verified by blocking SCV acidification. This reduces T2-*gfp* reporter induction by >32-fold in HeLa and MEF, the two key cell types used in our study (Figure S1A; Figure S3A). This blocking of T2-*gfp* expression by Bafilomycin is only effective, if the inhibitor is added before or at the time of infection. Adding it 2h p.i. or later diminishes the effect. This clearly shows that SCV acidification, a key environmental signal produced during SCV maturation, is essential for T2-*gfp* reporter induction.

Oher assays provide additional support, but are more tricky to interpret with respect to the requirement for SCV integrity, the time point of T2 expression, maturation or rupture. This is likely attributable to:

- the formation of T1-on and T1-off subpopulations
- the transient nature of the membrane damage (if repair occurs; see Figure S2A-D)
- the small size of the membrane which is below the resolution limit of the light microscopy techniques employed
- the difficulty of electron microscopy to follow membrane integrity in 3D-space
- the interpretation of beta-lactamase reporter assays in the face of multiple bacteria per cell
- the transient nature of breached SCV membranes and its relation to the access of cytosolic TEM substrates and/or cytosolic markers

Nevertheless, this type of assay provides additional support for the importance of SCV integrity for inducing T2-*gfp* expression:

Knockdown of Rab-GTPases promoting endosome to lysosome maturation (and which should not affect cytosolic bacteria) and of the vacuolar $H^+$-ATPase which drives endosome acidification (and which should not affect cytosolic bacteria) do significantly reduce T2-induction (Figure S1F, Figure S3C; Table S1B; (Misselwitz et al., 2011a)). This phenotype is less pronounced than that of bafilomycin. Nevertheless, these observations support that SCV maturation and acidification are promoting T2-induction.

*S*.Tm$^{SopE}$ bacteria expressing the T2-*gfp* reporter show little association with Ubiquitin (as a proxy for cytoplasmic access; Figure S1C, right panels; ≥ 80% of the T2-*gfp* expressing bacteria remain clear of Ubiquitin), but are strongly associated with LAMP-1 (Figure S1B; 80% of T2-*gfp* expressing bacteria stain positive for LAMP1 by 4h p.i.). The opposite is observed for bacteria which fail to express the T2-*gfp* reporter (Figure S1B) or "all" bacteria, which, in *atg5*$^{-/-}$ cells, mostly represent T2-off bacteria by 6h p.i. (Figure S1C, left panels). This changes dramatically, if we apply the osmotic shock procedure for just 13 minutes. After inflicting membrane damage by osmotic shock, T2-*gfp* expressing bacteria do associate with Ubiquitin much more frequently than in the control cells (Figure S6A,B). This is consistent with the T2-*gfp* expression being induced when *S*.Tm is lodged in an intact SCV. Some of these induced bacteria may subsequently leave the endosomal compartment. However, the majority of the T2-*gfp* expressing bacteria remain shielded from the cytoplasmic ubiquitination machinery by intact endosomal membranes. This machinery only gets access, if endosomal membranes are ruptured by osmotic shock.

Significant SCV damage in *S*.Tm$^{\Delta T1}$ infected cells, as detected by the fluid phase dye-dextran marker assay, was only observed after infliction of osmotic membrane damage. The dye was well-retained in the absence of T1, in particular in *atg5*$^{+/+}$ cells. In contrast, the dye was released when we applied the osmotic shock procedure (Figure 7B,C). This went along with a significant increase in the Ubiquitin-association with the T2-*gfp* expressing *S*.Tm$^{\Delta T1}$ (Figure S6B). This provides further evidence that the SCV membrane is indeed initially intact, but can be compromised by either T1- or osmotic shock inflicted damage.

We performed correlative light/electron microscopy. These experiments confirmed that bacteria expressing the T2-*gfp* reporter are indeed lodged in an SCV. However, as it is technically challenging to demonstrate unequivocally that the SCV membrane is truly continuous in all 3 dimensions, we could only gain indirect evidence for SCV membrane integrity. The integrity of the SCV membrane enclosing T2-*gfp* expressing bacteria in unperturbed HeLa cells could be inferred from the absence of cytoplasmic material in the lumen of the endosome. An illustrative example is presented in the Figure S1D.

Together, these lines of evidence confirm that T2-expression is indeed induced within intact endosomes when they mature into SCV.

Finally, it is important to note that our assays are set up in a fashion which does not require that every single GFP-positive bacterium is indeed enclosed by a late endosomal membrane. The steps of SCV maturation, endosome membrane damage and autophagy are (as a good approximation) stochastic processes whose likelihoods are affected by the host cellular trafficking pathways, the pathogen's virulence factors and autophagy-promoted endosome repair. The same is true for the nature of bacterial gene expression which occurs (largely) in response to the environmental signals perceived in the SCV lumen. Thus, it is well possible that a few GFP-positive bacteria can end up in the host cellular cytosol or that some bacterial cells are leaving the SCV and retain the stable GFP reporter when they arrive in the cytosol. Nevertheless, the available data clearly shows that the bulk of the GFP-positive bacteria do emerge in response to the environmental cues perceived by *S*.Tm residing in intact SCV. The single cell data that we provide reflects this stochastic nature of the T2-induction and careful statistical analysis has allowed to work out the role of autophagy.

**Microscopy of screening plates**

The 384-well screening plates were imaged in an automated manner using the Molecular Devices ImageXpress microscope. Robotic plate handling was used to load and unload the plates. The objective used for acquisition was a 10X S Fluor with 0.45NA. 9 sites per well were imaged in a 3x3 grid without spacing or overlap of the images using three channels for monitoring the cell's nuclei (DAPI stain), the cell's actin cytoskeleton (DY-547-phalloidin) and the GFP-expressing *S*.Tm (pM975).

**Image analysis of screening plates**

All data generated during InfectX related screens - including raw and processed image data - are shared through the openBIS biology information system (Bauch et al., 2011). To achieve an efficient automated image-analysis pipeline applicable to the distinct screening features exploited by the pathogens of the InfectX consortium, an open-source workflow management based on CellProfiler was developed (Rouilly et al., 2012). This workflow manager can modularly apply all required image analysis steps in an efficient fashion. To allow for quantitative assessment of a very broad set of cellular and subcellular features on several segmented cellular compartments, several novel or enhanced image analysis and data normalization modules based on CellProfiler (Carpenter et al., 2006) have been implemented into a modular and generic image analysis framework. The analysis involved image correction through shading correction of images before object detection using CellProfiler. First, the "Nuclei" were detected in the DAPI channel using the IdentifyPrimAutomatic module of CellProfiler. In a second step, the "PeriNuclei" were defined by an eight pixel comprising extension of the nucleus objects and the CellProfiler modules ExpandOrShrink and IdentifyTertiary were used to remove the nuclear area from this extended region. The "Cell" was identified using the actin cytoskeleton surrounding the nucleus object (actin channel) using the BeeIdentifySecondaryInformed module. In addition, we used an actin-independent strategy through the extension of 25 pixels from the nucleus ("Voronoi Cells"). On all four segmented objects (Nuclei,

PeriNuclei, Cells, Voronoi Cells), more than 500 distinct features involving spatial, intensity, and texture measurements were extracted out of 1.8 million images and in total more than 100 million cells. To detect the cells that were infected by *S*.Tm$^{SopE}$, a wavelet-based object detection was used to segment the GFP-dots that compose candidate locations of bacteria within the host cell. On the segmented bacteria candidates, a novel CellProfiler module (BeeMeasureObjectSubCell) was used to measure spatial features and the GFP intensity, resulting in a quantitative assessment of *S*.Tm$^{SopE}$ infection. To discriminate and remove false positives of segmented bacterial objects, a classification method based on a decision tree classifier has been applied. The decision tree classification has been optimized by a human expert, who identifies true internalized bacteria, and labels the parent cells as infected. This is the standard method to detect infection, applied to our presented data. To achieve best possible quality control of automated image-analysis for the siRNA screens, a second method to score infection was applied. Here, infected cells were identified via CellClassifier (Ramo et al., 2009) using supervised machine-based learning by a Support Vector Machine-(SVM) based classifier. As readout, the infection index defined the number of infected cells divided by the total numbers of cells in a well. To correct for potential plate- or batch effects within siRNA screens, a non-control based z-scored data normalization was performed to normalize for variations between distinct plates. After plate z-scoring, the whole screen was z-score normalized in order to facilitate screen-wide data analysis.

**Phenotypic clustering of the hits**

KEGG pathway analysis (Luo and Brouwer, 2013) was performed in order to phenotypically cluster and map the strongest negative 5000 hits of the genome-wide siRNA screen (z-score of cells harboring T2-*gfp*$^+$ *S*.Tm ≤ -0.5; corresponding to ≥ 30% decrease) according to their functional annotation.

**Binding assay**

The binding assay has been recently described (Misselwitz et al., 2011b). Briefly, 4.000 cells (*atg5*$^{+/+}$ and *atg5*$^{-/-}$) were seeded one day prior to experiment into "half-size" 96-well plates (Greiner Bio One). Cells were infected with *S*.Tm$^{\Delta 4}$ at an MOI=125 for 6min at 37°C and 5% $CO_2$. This non-invasive mutant strain allows to measure the binding capacity of *S*.Tm. Afterwards, the cells were washed 3x with 60µl DMEM/10%FCS and fixed with 60µl 4% PFA. To visualize bound *S*.Tm$^{\Delta 4}$, immunofluorescence staining was performed using a primary anti-LPS antibody (Difco) and a FITC-conjugated secondary antibody (Jackson). Afterwards, cells were permeabilized and the nuclei were stained with DAPI. Image analysis was performed using CellProfiler-based Matlab scripts detecting the cell's nuclei and the bacterial GFP dots (Misselwitz et al., 2011a; Misselwitz et al., 2011b).

**Quantification of Membrane Ruffles**

To manually quantify *S*.Tm-induced membrane ruffles on the host cell surface, 40.000 cells (*atg5*$^{+/+}$ and *atg5*$^{-/-}$) were seeded in 24-well plates (TPP) containing glass cover slips one day prior to infection. Cells were infected with 100µl *S*.Tm$^{SopE}$ (pM965; MOI=80) for 12min. Afterwards, the cells were washed 2x with PBS and fixed for 15min with 4% PFA. The cells were permeabilized with 0.1% Triton-X100 for 5min and then stained with DAPI and Tritc-Phalloidin (1µg/ml; Sigma) for 1h at RT. Quantification of induced membrane ruffles was achieved through the acquisition of z-stacks with a 100x-objective of the Zeiss Axiovert 200m inverted microscope. The fraction of cells with ruffles/total number of cells were quantified in a blinded fashion using the acquired image sections.

**Classical gentamicin-protection assay**

40.000 cells were seeded one day before infection into 24-well plates (TPP). The cells were infected with the respective *S*.Tm strains at a low MOI (~10) for 20min. Afterwards, the cells were washed 3x with DMEM/10% FCS and incubated with DMEM/10% FCS containing 400µg/ml gentamicin. At the indicated times after infection (1hpi - 6hpi), the cells were washed 3x with PBS and then lysed with PBS containing 0.1% Deoxycholic acid. Serial dilutions were made with the lysed cell suspension in PBS. 50µl of the diluted cell suspensions were plated on LB agar containing the appropriate antibiotics. Colony forming units (cfu's) were enumerated after overnight incubation at 37°C. Gentamicin-protection assays with the *S*.Tm$^{\Delta T1}$ mutant expressing the *Yersinia pseudotuberculosis* Invasin were performed at an MOI=40 (to partially compensate for its lower invasion

capacity). A helped infection was performed with the helped *S*.Tm$^{\Delta T1}$ mutant (MOI=40) and the "helper" *S*.Tm$^{SopE}$ (MOI=8). To determine the cfu's of both strains, differential plating on the appropriate antibiotics was performed.

**_gfp_-reporter assay for the *S*.Tm$^{\Delta T1}$ mutant**

In case the *gfp*-reporter assay was performed as a "helped" infection, the non-invasive mutant strain *S*.Tm$^{\Delta T1}$ (MOI=150-250; harbors the *gfp*-reporter plasmid) and its respective "helper" strain *S*.Tm$^{SopE}$ (MOI=40-60) were mixed prior to infection and then added to the host cells. The infection period was extended from 20min to 60min. After additional 3h of incubation in presence of gentamicin-containing medium, the cells were fixed with 4% PFA. Staining, microscopy and analysis was done as described above (*S*.Tm infection of siRNA screening plates).

**Inhibitor treatment**

Bafilomycin (200nM; Enzo Life Science) was diluted in DMEM/10% FCS and added to the cells at the indicated time points before or during infection with *S*.Tm.

**Lentiviral transduction of tissue culture cells**

One day before transduction, 7.000 cells were seeded in 24-well plates (TPP). On the next day, cells were washed 1x with PBS and replenished with fresh DMEM/10% FCS. Then, 2.5µg/ml Polybrene (Millipore) and the lentivirus (MOI=2.5) were sequentially added to each well. After 24h of incubation at 37°C and 5% $CO_2$, the medium was replaced by fresh medium and further incubated for 24-48h at 37°C and 5% $CO_2$.

**Chemical transfection and nucleofection of plasmids into tissue culture cells**

For the transient overexpression of plasmids through chemical transfection, cells were seeded one day before transfection. On the next day, 1µg of plasmid DNA was first incubated with transfection reagent for 15min (Lipofectamine 2000 or RNAiMAX; Invitrogen) and then added dropwise to the cells. 3h after transfection, the medium was replaced with DMEM/10% FCS. After 24-48h, the experiment (infection, microscopic sampling) took place. For enhanced expression of plasmids in *atg5*$^{+/+}$ and *atg5*$^{-/-}$ cells, nucleofection with the MEF Nucleofector Kit 1 (Amaxa) was performed as recommended by manufacturer.

**Statistics**

The number of biological replicates was sufficient to perform statistics using the non-parametric Mann-Whitney U test, comparing individual data points for experimental- and control samples.

**Fluorescence microcopy and quantitative analysis of co-localization**

The cells (HeLa cells, *atg5*$^{+/+}$ and *atg5*$^{-/-}$ MEFs) were seeded on coverslips in 24-well plates (TPP) one day prior to the experiment. At the end of the assay, cells were fixed for 15min with 500µl 4% PFA and then permeabilized with 0.1% TritonX-100 (Sigma) for 5min at RT. Cells were first incubated with blocking buffer for 30min and then stained using the appropriate antibodies. The coverslips were then mounted with 5µl Mowiol (Sigma). Image acquisition was performed with the 100x-objective using the Zeiss Axiovert 200m inverted microscope with a Yokogawa CSU-X1 spinning-disk confocal unit (Visitron) and a PLAN- Apochromat 100x oil objective with an aperture setting of 1.3 (Zeiss). To quantify co-localizations of host proteins with intracellular *S*.Tm, the quantitation module of Volocity was used. Here, the intensity of each individual bacterium was measured and then normalized to the background intensity in close proximity to the measured bacterium to achieve optimal normalization with reference to the respective background intensities. The detection threshold in the absence of measurable co-localizations was set to "zero".

**Correlative light/electron microscopy**

HeLa cells were grown in a 10cm dish and infected with *S*.Tm$^{SopE}$ at an MOI=50 for 25min at 37°C in EM buffer (120 mM NaCl, 7 mM KCl, 1.8 mM $CaCl_2$, 0.8 mM $MgCl_2$, 5 mM glucose, 25 mM HEPES, pH 7.3). Cells were washed 3x with EM, then placed in EM + 10% FBS + gentamycin 100 for 1h, at which point the media was switched to EM +10% FBS + gentamycin 10. At 4 h p.i., cells were rinsed once in EM and then fixed for 10min at RT in 2% PFA (EMS) + 0.05% glutaraldehyde in PHEM buffer (60 mM PIPES, 25mM HEPES, 10 mM EGTA, 2 mM MgCl2, pH 7.3). Fixative was then switched to 2% PFA in PHEM buffer for 1h. Cells were prepared for EM according to standard

Tokuyasu techniques (Oorschot et al., 2014). Briefly, before scraping, free aldehydes were quenched with 50 mM $NH_4Cl$ in PBS and the cell pellet was embedded in 12% gelatine (TAAB). After solidification of the gelatine, blocks of 1 $mm^3$ were cut and infiltrated overnight with 2.1 M sucrose in PBS at 4°C. Blocks were mounted on pins and frozen by plunging in liquid nitrogen. Thin sections were cut with a thickness of 75 nm using a Leica UC6/FC6 (Leica microsystems) at -120°C. Sections were collected on HF 15 finder grids (Agar) coated with a formvar and carbon film. Labeling for fluorescence was done according to Oorschot et al. (2014) using a rabbit anti GFP (Rockland, 1:100 in PBS + 1% BSA) and mouse anti lamp1 (BD Pharmigen, 1:100 in PBS +1% BSA) followed by anti-mouse Cy3 and anti-rabbit AlexaFluor 488 (both Molecular Probes, 1:200 in PBS +1% BSA). Grids were then washed with PBS and water and stained with Hoechst (Molecular Probes, 1:1000 in water). After rinsing, grids were mounted on slides using 50% glycerol and imaged using a Perkin Elmer UltraView spinning disc confocal microscope, with a 60X/ 1.2NA water objective. After fluorescence imaging, sections were contrasted with 0.4% uranylacetate (Merck) in 1.8 methylcellulose and cells of interest were observed with a Tecnai G2 (FEI) run at 120kV equipped with a US 4000 (Gatan). Alignment of EM and LM images was performed using Amira software (FEI).

**Expulsion Assay**

The expulsion assay was performed as described (Miao et al., 2015). *atg5*$^{+/+}$ and *atg5*$^{-/-}$ cells were seeded in 24-well dishes and infected with *S*.Tm$^{SopE}$ at an MOI=100. After 20min, cells were washed 2x and treated with gentamicin-containing medium for 1h to kill extracellular *S*.Tm. At this time point, three wells from each cell line were washed and permeabilized (as indicated for the gentamicin-protection assay) to recover the initial bacterial loads. The remaining wells were replenished with fresh medium containing trimethoprim (25µg/ml; Sigma) and α-methyl-mannose (100mM). At 4h.40 and 6h.40 p.i., culture supernatant (50µl) was collected from each well and plated on LB agar plates to recover expelled bacteria.

**Fluid-phase marker analysis using FITC-dextran**

One day before experiment, 70.000 cells were seeded in 24-well plates (TPP). 1mg/ml of FITC-dextran (TdB consultancy, 500kDa) in DMEM/10%FCS was added to *atg5*$^{+/+}$ and *atg5*$^{-/-}$ cells together with *S*.Tm$^{SopE}$ (pWRG435, MOI=40) during an infection time of 20min or with a helped infection of *S*.Tm$^{\Delta T1}$ (pWRG435, MOI=120, *S*.Tm$^{SopE}$ =unlabeled helper) during an infection time of 60min. Afterwards, cell were washed twice and DMEM/10%FCS containing 400µg/ml gentamicin was added. At 90min post infection, cells were washed twice with PBS and then fixed for 15min with 4%PFA at RT. Extracellular *S*.Tm were stained with an anti-LPS antibody (CY5). Afterwards, cells were permeabilized and the nuclei were stained with DAPI. The remaining steps and analysis were performed as described in Fluorescence Microscopy.

**Fluid-phase marker analysis using Blue-dextran after osmotic damage**

Two days before the experiment, *atg5*$^{+/+}$ and *atg5*$^{-/-}$ cells were transfected with the Galectin-3-mOrange overexpression plasmid. 1mg/ml Blue-dextran (TdB consultancy, 500kDa) in DMEM/10%FCS was added to *atg5*$^{+/+}$ and *atg5*$^{-/-}$ cells together with *S*.Tm$^{\Delta T1}$ (pM965; constitutive GFP; MOI=120) through HGF-(10ng/ml) induced internalization for 60min. At this time point, endosomal damage was performed as described before (Thurston et al., 2012). Briefly, cells were exposed to hypertonic medium (0.5M sucrose in PBS, with or without 10% PEG1000) for 10min at 37°C, washed twice with PBS and then incubated in 60% PBS for 3min at 37°C. Afterwards, cells were recovered in fresh medium (DMEM+10%FCS) for 20min at 37°C and then fixed and stained for extracellular bacteria as described above.

# Supplemental References


Bauch, A., I. Adamczyk, P. Buczek, F.J. Elmer, K. Enimanev, P. Glyzewski, M. Kohler, T. Pylak, A. Quandt, C. Ramakrishnan, C. Beisel, L. Malmstrom, R. Aebersold, and B. Rinn. 2011. openBIS: a flexible framework for managing and analyzing complex data in biology research. *BMC bioinformatics* 12:468.

Bender, J.K., T. Wille, K. Blank, A. Lange, and R.G. Gerlach. 2013. LPS structure and PhoQ activity are important for Salmonella Typhimurium virulence in the Galleria mellonella infection model [corrected]. *PloS one* 8:e73287.

Carpenter, A.E., T.R. Jones, M.R. Lamprecht, C. Clarke, I.H. Kang, O. Friman, D.A. Guertin, J.H. Chang, R.A. Lindquist, J. Moffat, P. Golland, and D.M. Sabatini. 2006. CellProfiler: image analysis software for identifying and quantifying cell phenotypes. *Genome biology* 7:R100.

Diard, M., V. Garcia, L. Maier, M.N. Remus-Emsermann, R.R. Regoes, M. Ackermann, and W.D. Hardt. 2013. Stabilization of cooperative virulence by the expression of an avirulent phenotype. *Nature* 494:353-356.

Ehrbar, K., A. Friebel, S.I. Miller, and W.D. Hardt. 2003. Role of the Salmonella pathogenicity island 1 (SPI-1) protein InvB in type III secretion of SopE and SopE2, two Salmonella effector proteins encoded outside of SPI-1. *Journal of bacteriology* 185:6950-6967.

Ehsani, S., J.C. Santos, C.D. Rodrigues, R. Henriques, L. Audry, C. Zimmer, P. Sansonetti, G. Tran Van Nhieu, and J. Enninga. 2012. Hierarchies of host factor dynamics at the entry site of Shigella flexneri during host cell invasion. *Infection and immunity* 80:2548-2557.

Hapfelmeier, S., K. Ehrbar, B. Stecher, M. Barthel, M. Kremer, and W.D. Hardt. 2004. Role of the Salmonella pathogenicity island 1 effector proteins SipA, SopB, SopE, and SopE2 in Salmonella enterica subspecies 1 serovar Typhimurium colitis in streptomycin-pretreated mice. *Infection and immunity* 72:795-809.

Hapfelmeier, S., B. Stecher, M. Barthel, M. Kremer, A.J. Muller, M. Heikenwalder, T. Stallmach, M. Hensel, K. Pfeffer, S. Akira, and W.D. Hardt. 2005. The Salmonella pathogenicity island (SPI)-2 and SPI-1 type III secretion systems allow Salmonella serovar typhimurium to trigger colitis via MyD88-dependent and MyD88-independent mechanisms. *Journal of immunology* 174:1675-1685.

Hardt, W.D., L.M. Chen, K.E. Schuebel, X.R. Bustelo, and J.E. Galan. 1998. S. typhimurium encodes an activator of Rho GTPases that induces membrane ruffling and nuclear responses in host cells. *Cell* 93:815-826.

Hoffmann, C., M. Galle, S. Dilling, R. Kappeli, A.J. Muller, P. Songhet, R. Beyaert, and W.D. Hardt. 2010. In macrophages, caspase-1 activation by SopE and the type III secretion system-1 of S. typhimurium can proceed in the absence of flagellin. *PloS one* 5:e12477.

Hoiseth, S.K., and B.A. Stocker. 1981. Aromatic-dependent Salmonella typhimurium are non-virulent and effective as live vaccines. *Nature* 291:238-239.

Kaniga, K., J.C. Bossio, and J.E. Galan. 1994. The Salmonella typhimurium invasion genes invF and invG encode homologues of the AraC and PulD family of proteins. *Molecular microbiology* 13:555-568.

Kuma, A., M. Hatano, M. Matsui, A. Yamamoto, H. Nakaya, T. Yoshimori, Y. Ohsumi, T. Tokuhisa, and N. Mizushima. 2004. The role of autophagy during the early neonatal starvation period. *Nature* 432:1032-1036.

Luo, W., and C. Brouwer. 2013. Pathview: an R/Bioconductor package for pathway-based data integration and visualization. *Bioinformatics* 29:1830-1831.

Miao, Y., G. Li, X. Zhang, H. Xu, and S.N. Abraham. 2015. A TRP Channel Senses Lysosome Neutralization by Pathogens to Trigger Their Expulsion. *Cell* 161:1306-1319.

Mirold, S., K. Ehrbar, A. Weissmuller, R. Prager, H. Tschape, H. Russmann, and W.D. Hardt. 2001. Salmonella host cell invasion emerged by acquisition of a mosaic of separate genetic elements,

including Salmonella pathogenicity island 1 (SPI1), SPI5, and sopE2. *Journal of bacteriology* 183:2348-2358.

Misselwitz, B., N. Barrett, S. Kreibich, P. Vonaesch, D. Andritschke, S. Rout, K. Weidner, M. Sormaz, P. Songhet, P. Horvath, M. Chabria, V. Vogel, D.M. Spori, P. Jenny, and W.D. Hardt. 2012. Near surface swimming of Salmonella Typhimurium explains target-site selection and cooperative invasion. *PLoS pathogens* 8:e1002810.

Misselwitz, B., S. Dilling, P. Vonaesch, R. Sacher, B. Snijder, M. Schlumberger, S. Rout, M. Stark, C. von Mering, L. Pelkmans, and W.D. Hardt. 2011a. RNAi screen of Salmonella invasion shows role of COPI in membrane targeting of cholesterol and Cdc42. *Molecular systems biology* 7:474.

Misselwitz, B., S.K. Kreibich, S. Rout, B. Stecher, B. Periaswamy, and W.D. Hardt. 2011b. Salmonella enterica serovar Typhimurium binds to HeLa cells via Fim-mediated reversible adhesion and irreversible type three secretion system 1-mediated docking. *Infection and immunity* 79:330-341.

Muller, A.J., C. Hoffmann, M. Galle, A. Van Den Broeke, M. Heikenwalder, L. Falter, B. Misselwitz, M. Kremer, R. Beyaert, and W.D. Hardt. 2009. The S. Typhimurium effector SopE induces caspase-1 activation in stromal cells to initiate gut inflammation. *Cell host & microbe* 6:125-136.

Oorschot, V.M., T.E. Sztal, R.J. Bryson-Richardson, and G. Ramm. 2014. Immuno correlative light and electron microscopy on Tokuyasu cryosections. *Methods in cell biology* 124:241-258.

Paz, I., M. Sachse, N. Dupont, J. Mounier, C. Cederfur, J. Enninga, H. Leffler, F. Poirier, M.C. Prevost, F. Lafont, and P. Sansonetti. 2010. Galectin-3, a marker for vacuole lysis by invasive pathogens. *Cellular microbiology* 12:530-544.

Pelkmans, L., T. Burli, M. Zerial, and A. Helenius. 2004. Caveolin-stabilized membrane domains as multifunctional transport and sorting devices in endocytic membrane traffic. *Cell* 118:767-780.

Ramo, P., A. Drewek, C. Arrieumerlou, N. Beerenwinkel, H. Ben-Tekaya, B. Cardel, A. Casanova, R. Conde-Alvarez, P. Cossart, G. Csucs, S. Eicher, M. Emmenlauer, U. Greber, W.D. Hardt, A. Helenius, C. Kasper, A. Kaufmann, S. Kreibich, A. Kuhbacher, P. Kunszt, S.H. Low, J. Mercer, D. Mudrak, S. Muntwiler, L. Pelkmans, J. Pizarro-Cerda, M. Podvinec, E. Pujadas, B. Rinn, V. Rouilly, F. Schmich, J. Siebourg-Polster, B. Snijder, M. Stebler, G. Studer, E. Szczurek, M. Truttmann, C. von Mering, A. Vonderheit, A. Yakimovich, P. Buhlmann, and C. Dehio. 2014. Simultaneous analysis of large-scale RNAi screens for pathogen entry. *BMC genomics* 15:1162.

Ramo, P., R. Sacher, B. Snijder, B. Begemann, and L. Pelkmans. 2009. CellClassifier: supervised learning of cellular phenotypes. *Bioinformatics* 25:3028-3030.

Rouilly, V., E. Pujadas, B. Hullar, C. Balazs, P. Kunszt, and M. Podvinec. 2012. iBRAIN2: automated analysis and data handling for RNAi screens. *Studies in health technology and informatics* 175:205-213.

Stecher, B., S. Hapfelmeier, C. Muller, M. Kremer, T. Stallmach, and W.D. Hardt. 2004. Flagella and chemotaxis are required for efficient induction of Salmonella enterica serovar Typhimurium colitis in streptomycin-pretreated mice. *Infection and immunity* 72:4138-4150.

Thurston, T.L., M.P. Wandel, N. von Muhlinen, A. Foeglein, and F. Randow. 2012. Galectin 8 targets damaged vesicles for autophagy to defend cells against bacterial invasion. *Nature* 482:414-418.